NASA TECHNICAL MEMORANDUM

NASA TM X-3002

NASA TM X-3002

INSTANTANEOUS DISTORTION IN A MACH 2.5, 40-PERCENT-INTERNAL-CONTRACTION INLET AND ITS EFFECT ON TURBOJET STALL MARGIN

by Paul L. Burstadt and James E. Calogeras

Lewis Research Center
Cleveland, Ohio 44135

NATIONAL AERONAUTICS AND SPACE ADMINISTRATION • WASHINGTON, D. C. • JULY 1974

1. Report No. NASA TM X-3002	2. Government Accession No.	3. Recipient's Catalog No.
4. Title and Subtitle INSTANTANEOUS DISTORTION IN A MACH 2.5, 40-PERCENT-INTERNAL-CONTRACTION INLET AND ITS EFFECT ON TURBOJET STALL MARGIN		5. Report Date JULY 1974 6. Performing Organization Code
7. Author(s) Paul L. Burstadt and James E. Calogeras		8. Performing Organization Report No. E-6294 10. Work Unit No. 501-24
9. Performing Organization Name and Address Lewis Research Center National Aeronautics and Space Administration Cleveland, Ohio 44135		11. Contract or Grant No. 13. Type of Report and Period Covered Technical Memorandum
12. Sponsoring Agency Name and Address National Aeronautics and Space Administration Washington, D.C. 20546		14. Sponsoring Agency Code
15. Supplementary Notes		

16. Abstract

An experimental wind-tunnel investigation was conducted to determine the effects of time-variant distortions produced in a supersonic inlet on a J85-GE-13 turbojet engine. Results are presented principally in terms of "instantaneous" distortion amplitudes and total-pressure contours measured through compressor stall. They indicate that, although a time-averaged distortion may be far from a stall-inducing value, corresponding instantaneous distortion amplitudes can approach or exceed this value. Seven engine stall events were studied. In six of these events instantaneous distortion peaks of sufficient magnitude to cause stall were observed in the time period shortly before stall was detected.

17. Key Words (Suggested by Author(s))	18. Distribution Statement
Instantaneous distortion; Total pressure distortion; Stall margin; Compressor sensitivity to distortion; Inlet-engine compatibility	Unclassified - unlimited Category 28

19. Security Classif. (of this report)	20. Security Classif. (of this page)	21. No. of Pages	22. Price*
Unclassified	Unclassified	40	$3.25

* For sale by the National Technical Information Service, Springfield, Virginia 22151

INSTANTANEOUS DISTORTION IN A MACH 2.5, 40-PERCENT-INTERNAL-CONTRACTION INLET AND ITS EFFECT ON TURBOJET STALL MARGIN

by Paul L. Burstadt and James E. Calogeras

Lewis Research Center

SUMMARY

An experimental wind-tunnel investigation was conducted to determine the effects of time-varying total-pressure distortions produced in a supersonic inlet on a J85-GE-13 turbojet engine. Results are presented principally in terms of "instantaneous" distortion amplitudes and total-pressure contours measured through compressor stall. They indicate that although a time-averaged distortion may be far from a stall-inducing value, corresponding instantaneous distortion amplitudes can approach or exceed this value.

Seven engine stall events were studied. The time-varying data were averaged to account for engine response characteristics so that an existing steady-state distortion parameter and stall correlation could be applied on an instantaneous basis. When this was done, instantaneous distortion peaks of sufficient magnitude to cause stall were observed for six of the cases in the time period shortly before stall was detected. However, instantaneous distortion peaks of equal or greater magnitude were observed at earlier times. The fact that these earlier peaks did not cause stall indicates a lack of detailed understanding of the effects of distortion on compressor operation. For this reason, it was concluded that the instantaneous distortion approach discussed in this report might be used to determine a statistical probability of stall, but it does not provide an explicit indication of stall.

INTRODUCTION

Total-pressure fluctuations produced in a supersonic inlet are a major problem associated with inlet-engine compatibility. When considered at any instant, such time-variant pressures can result in a large airflow distortion at the inlet-engine interface relative to the time-averaged distortion. A major share of the fluctuations appear to originate from an unsteady interaction of the terminal shock with the diffuser boundary

layer. Time-variant distortion can seriously degrade compressor stall margin. Several experimental investigations have already verified both the cause and effect of time variant distortion (e.g., refs. 1 to 3). Further, such studies have qualitatively related the amount of stall margin degradation to the amplitude of the dynamic activity. But the preponderance of data thus far accumulated were recorded either in an environment of artifically created distortion dynamics or in the absence of an engine.

The present investigation was conducted in the 10- by 10-Foot Supersonic Wind Tunnel of the NASA Lewis Research Center. Its purpose was to measure time-variant distortions produced in a supersonic inlet just before compressor stall. An axisymmetric, mixed-compression inlet designed for Mach 2.5 was coupled to a J85-GE-13 turbojet engine. Steady-state and dynamic data were recorded over a range of operating conditions at Mach numbers of 2.5, 2.6, and 2.7. Results are presented principally in terms of "instantaneous" distortion amplitudes and total-pressure contours measured for several compressor stalls. The instantaneous distortion amplitudes are compared with a steady-state distortion correlation to see if instantaneous distortion levels can be identified as the cause of stall. Compressor-face total-pressure contours are shown for each stall, and the relation between steady-state, instantaneous, and rms total-pressure variations is discussed.

SYMBOLS

DPCWR	distortion index (defined in RESULTS AND DISCUSSION)
LSPR	loss in stall compressor pressure ratio (defined in RESULTS AND DISCUSSION)
M	Mach number
m	mass flow
N	engine speed, rpm
N^*	rated engine speed, 16 500 rpm
$\frac{N \times 100}{N^* \sqrt{\theta_2}}$	corrected engine speed, percent
P	total pressure, N/m^2 (lbf/ft^2)
ΔP	fluctuating component of total pressure
p	static pressure, N/m^2 (lbf/ft^2)
T	total temperature, K (^oR)
W	engine airflow, kg/sec (lbm/sec)

W_{corr}	corrected engine airflow, $W\sqrt{\theta}/\delta$, kg/sec (lbm/sec)
α	angle of attack, deg
β	spoiled sector angle, deg
δ	local corrected total pressure, $P/101\ 325\ N/m^2$ ($P/2116\ lbf/ft^2$)
θ	local corrected total temperature, $T/288.2\ K$ ($T/518.7^{\circ}\ R$)
σ	standard deviation
τ	data averaging period; averaging time (sec) $\times$ N/(60 sec/min), rotor revolutions

Subscripts:

0	free stream
2	compressor-face station
2.1	compressor first stage exit station
2.2–2.7	etc.
3	compressor discharge station
min, 60°	minimum value in a 60° sector of station 2
ring	inner or outer annulus of station 2

Superscript:

$\bar{}$	spatial average

APPARATUS AND PROCEDURE

Inlet Description

The inlet used in this investigation was designed for Mach 2.5 and sized to match the airflow requirements of a J85-GE-13 engine. A photograph of the inlet terminated by a coldpipe-choked plug assembly is shown in figure 1 mounted in the wind tunnel. Some of the more pertinent details are illustrated in figure 2; more complete inlet design and performance details are given in reference 4. The inlet was an axisymmetric mixed-compression type with 40 percent of the supersonic flow area contraction provided internally. This was accomplished with a biconic centerbody that was translated to effect inlet start and off-design operation. Internally, the cowl lip shock was cancelled at its impingement point on the centerbody. Further isentropic compression resulted in a throat Mach number of 1.30. Provisions were made for both boundary-layer bleed and vortex generators on cowl and centerbody surfaces in the region of the geometric throat.

The compressor-face station was segmented by three centerbody support struts, which extended forward about half the length of the subsonic diffuser. Each of the three duct segments contained two ejector and two overboard bypasses which provided engine cooling and off-design airflow matching, respectively. Both the ejector and overboard bypasses were located in a common cavity. A dual-vane cascade was installed at the entrance to each cavity to alleviate a resonance associated with these volumes (ref. 5).

Engine Description

The General Electric J85-GE-13 is an afterburning turbojet with a high thrust-to-weight ratio. The engine consists of an eight-stage axial-flow compressor coupled to a two-stage turbine. It incorporates controlled compressor interstage bleed and variable inlet guide vanes, a throughflow annular combustor, and an afterburner (not used in this test) with a variable area primary exhaust nozzle. The engine inlet diameter is 40.9 centimeters (16.1 in.).

The exhaust nozzle area was manually controlled for this investigation. The compressor was stalled by slowly closing the nozzle while maintaining a constant engine speed. To avoid exceeding the turbine temperature limit during this procedure, the first-stage turbine nozzle area was approximately 14 percent smaller than the standard nozzle. This meant that at any point on the compressor map the turbine was matched to the compressor at a lower turbine-inlet temperature. Compressor interstage bleed, mechanically linked to the inlet guide vanes, was scheduled linearly from fully closed at 90 percent of corrected engine speed to fully open at 76 percent of corrected speed. This was considered to be the limit of safe deviation from the normal schedule, which varied between 94 and 80 percent of corrected speed. This modified schedule made the compressor operate with less than normal stall margin.

Instrumentation

Steady-state and dynamic pressure instrumentation at the compressor face and compressor discharge stations is shown in figure 3(a). Only the fluctuating component of pressure was recorded from each of the dynamic probes. Absolute pressures were later obtained by adding the fluctuating component to the steady-state value provided by the adjacent probe. An additional correction was made at this time to account for leakage of the high-pass filters, which had caused a small zero-shift of the fluctuating signals. Frequency response of the dynamic probes at the compressor face was flat to about 2000 hertz. Response of the compressor discharge dynamic probes and the interstage static probes shown in figure 3(b) was flat to about 300 hertz.

Acquisition and Reduction of Data

A block diagram of the analog data acquisition system is shown in figure 4(a). The fluctuating signal from each pressure transducer was recorded on FM-multiplexed tape at 152.4 centimeters per second (60 in./sec). This speed provided recording capability of up to 4000 hertz.

Figure 4(b) is a block diagram of the data reduction system for the 30 compressor-face total pressures. The FM tape was played back at 9.525 centimeters per second (3.75 in./sec), or 1/16 of the original recording speed. Signals from the tape were demultiplexed and then passed through a bank of linear-phase amplifier-filters. Gain settings were selected to provide the correct ranges for the digitizer, and bandwidth settings were selected to provide low-pass filtering at an effective frequency of 1600 hertz (i.e., 16 times the bandwidth setting). The data in a 225-millisecond period (about 215 msec before stall) were then digitized at an effective rate of 8000 points per second per channel and put on tape. This digitizing rate provided five points per cycle of the highest frequency signal that passed through the amplifier-filters.

Calculations were made for each time slice generated by the digitizer. Reduced data were then provided in the form of microfilm plots and/or printed output.

The rms amplitude of the fluctuating component of total pressure was determined for each of the compressor-face dynamic probes. This was done on-line by passing the dynamic signals through low-pass filters with 1000-hertz corner frequencies, and then measuring them with true rms (trms) meters. The output of each meter was then recorded on the steady-state data system after passing through another low-pass filter with a corner frequency of 1/24 hertz.

Dynamic data from the compressor interstage and discharge measuring stations were not processed through the reduction system shown in figure 4(b) but were reduced to the form of oscillograph traces, using the linear-phase amplifier-filters.

Data Bank

A description of the set of stall events recorded in this program is shown in figure 5. For many of the stalls the event recorded on FM tape and the corresponding steady-state data scan were recorded at slightly different operating conditions. The test procedure was to establish an engine operating condition in the vicinity of the compressor-stall point. The FM tape recorder was started and a steady-state data scan was made. Then, while the FM tape recorder was still running, the compressor pressure ratio was increased slightly and the throttle adjusted to maintain a constant rotor speed (see Engine Description). If stall did not occur, this procedure was repeated until the stall event

was recorded on the FM tape. In some cases the stall occurred after the engine had stabilized at an equilibrium operating condition. These were called "drift" stalls.

Seventeen of the 29 stalls recorded were of the "drift" type, and in 11 cases a steady-state data scan had been completed immediately before stall. These 11 cases provided the most accurate data for determining distortion values, and for this reason they were the only cases examined in detail. Two of these 11 cases had relatively low levels of both steady-state and dynamic, $\overline{(\Delta P_{rms}/\overline{P})}_2$, distortion. As a result, they showed very little loss in stall margin. Two other cases showed significant losses in stall margin, but the dynamic level was low, and the loss was attributed to their respective steady-state distortion levels. So of the 29 stall events recorded on tape, only seven were determined to be suitable for instantaneous distortion analysis.

RESULTS AND DISCUSSION

Steady-State Compressor Performance

Compressor performance with both undistorted and hub-radial distorted inflows is presented in figure 6. The stall compressor-pressure ratios from these figures are shown in figure 7 as a function of corrected engine speed. These data were recorded in an altitude test facility as part of a program to determine the effect of steady-state total-pressure distortions on a J85-GE-13 turbojet (see ref. 6). The same engine was used in the wind tunnel test program discussed herein, so that correlations from the steady-state program could be applied without considering engine-to-engine variations.

Figure 7 is the basis for determining the loss in stall compressor pressure ratio (LSPR) suffered by the engine at any stall point. The compressor map for hub-radial distortion is substantially different from either the undistorted map or those resulting from circumferentially distorted inflows shown in reference 6. For this reason it was decided to base LSPR on the dashed curve of figure 7, whenever steady-state hub-radial distortion was present, and on the solid curve for all other cases. Then LSPR is defined as:

$$\text{LSPR} \equiv \left[1 - \frac{\overline{P}_3/\overline{P}_2 \text{ distorted stall}}{\overline{P}_3/\overline{P}_2 \text{ ref}}\right]_{\frac{N}{N^*\sqrt{\theta_2}} = \text{constant}}$$

where $(\overline{P}_3/\overline{P}_2)_{ref}$ is from figure 7.

Steady-State Compressor Sensitivity to Stall

The sensitivity of the compressor to various types of steady-state distortion patterns is presented in figure 8. These results are from the screen-induced distortion program reported in reference 6. Loss in stall compressor pressure ratio is plotted as a function of a distortion index based on a critical angle of spoiled flow. This index, DPCWR, was developed from the test results of reference 9 and is determined from the two inner rings and two outer rings of compressor-face total-pressure probes shown in figure 3(a).

A simple radial averaging procedure is used to convert the 12 pressures in the two inner rings into an equivalent set of six pressures, each representing a 60° sector. The same procedure is then applied to the two outer rings. The distortion is then calculated for each (inner and outer) equivalent ring as

$$\text{distortion} = \left(1 - \frac{P_{\min,60^{\circ}}}{\overline{P}}\right)_{\text{ring}} \sqrt{\frac{\beta_{\text{ring}}}{180^{\circ}}}$$

where

$\overline{P}$ ring average pressure

$P_{\min,60^{\circ}}$ minimum pressure in ring

β_{ring} 60° times number of contiguous pressures in ring less than $\overline{P}$

The maximum of these two distortion values is called DPCWR.

The data in figure 8 represent stall points for each of the patterns shown. The distortion index takes no direct account of pure radial distortions. But the effect of hub-radial distortions is considered in the definition of LSPR, as mentioned previously. Midspan radial distortions had little effect on compressor performance, and they were neglected in the definition of DPCWR. Tip-radial distortions did affect compressor performance, but the effect was not considered since an accurate correlation was not available.

In figure 8 the rms error, or one standard deviation σ, of the DPCWR values with respect to the faired curve was determined to be 0.01. For random data scatter the ± 0.01 band would include 68 percent of the data points. So when a value of DPCWR is determined from a given value of LSPR, an error band of at least ± 0.01 must also be considered. This error band can be quite large in terms of percent for small values of DPCWR. However, we will be considering only the absolute value of the error band when discussing the accuracy of a correlation between instantaneous distortion levels and compressor stall.

Description of the Seven Drift Stalls

Inlet-engine operating conditions are listed in table I for the seven drift stalls to be analyzed. The predicted critical distortion in table I (also referred to as the critical level) is the value of DPCWR from figure 8 corresponding to the value of LSPR, which accounts for hub-radial distortion as discussed previously. It is the value of distortion index predicted to be necessary to cause the measured LSPR and has an associated error band of ±0.01, as discussed earlier.

The average rms amplitude of the fluctuating component of total pressure is also shown in table I. Each of the values recorded from the trms meters (see Acquisition and Reduction of Data) was divided by $\bar{P}_2$, and then an average of all 30 ratios was computed.

Steady-state operating points for the seven drift stalls are shown plotted on a compressor map in figure 9. The speed characteristics for undistorted inflow are shown as dashed lines. Corrected speed values for the stall points are listed in table I.

A series of compressor-face total-pressure contours for each of the seven drift stalls is shown in figure 10. The contours represent the steady-state, dynamic (i.e., rms), and instantaneous total pressures. They were made by fitting a surface through the 30 individual pressure values and then assigning shadings to different ranges. Although the aft section of the subsonic diffuser was segmented by three centerbody support struts, they were ignored when the contours were made. The instantaneous total-pressure contours correspond to high levels of instantaneous distortion and will be discussed in conjunction with subsequent figures. They are included in figure 10 for ease of comparison with the steady-state contours.

The descriptions of the steady-state distortion patterns given in table I can be seen from examination of figure 10. Contours of the fluctuating component of total pressure (rms) indicate that the highest level of dynamic activity (dark shading) generally occurred in a band between the high and low total-pressure regions. This band corresponds to a region with large spatial total-pressure gradients. These regions of high dynamic activity are strongly related to the instantaneous distortion amplitudes that preceeded compressor stall.

Determination of Time of Stall

To evaluate the results of the instantaneous distortion analysis, it was necessary to have an accurate indication of the time when stall occurred inside the compressor. The signals from the compressor static-pressure transducers (see fig. 3(b)) were put out on strip charts and examined. For all seven drift stalls the row of instrumentation at the 290° location showed the earliest indication of stall and these are the charts shown in figure 11. Since the origin of a stall zone in a compressor stage causes an abrupt loss

in the airflow pumping of that stage, a compression wave is sent forward and an expansion wave is sent rearward. Previous investigations with the J85 (ref. 7) have indicated that stall originates in a circumferential sector of the compressor. The stalled sector then increases in circumferential extent as it rotates in the same direction as the rotor, but at about half rotor speed. Results indicate that, in general, the stall zone makes one or two complete revolutions before terminal flow breakdown occurs, causing the rapid rise in inlet total-pressure known as the hammershock. This means that the hammershock cannot be used as an accurate indication of the stall time, since the period between the first indication of stall and the hammershock is variable.

Because there were only two axial rows of instrumentation inside the compressor, it was not possible to determine exactly when stall originated inside the compressor. Although the first indication was seen at the 290° location, a stall zone could originate just past the 45° location but not be detected until it rotated past the instrumentation at 290°. Since the stall zone rotated at about half rotor speed (8 msec/rev) there could be as much as a 6-millisecond delay before it was detected at the 290° location. This possible time delay will be important when discussing the instantaneous analysis in later figures.

Figure 11(a) shows that for reading 141, stall was first observed inside the compressor at 43 milliseconds. (The zero of the time scales corresponds to the start of instantaneous distortion calculations.) Static pressure rose at the exit of stages 1 and 2, and pressure dropped at the exit of stages 4 through 7. (The initial disturbance is not clearly shown at the stage 3 exit.) This indicates a stall zone which originated in stage 3 or 4. Complete flow breakdown occurred at about 50 milliseconds.

Charts for the other six readings are shown in the remaining sections of figure 11. In some cases the initial indication of stall is not as obvious as the disturbance caused by the second passage of the stalled zone. Figure 11(e) is an example of this situation. The first and third stages show small disturbances at about 36 milliseconds. Since stronger disturbances were observed about 7 to 8 milliseconds later (the time required for one rotation of the stalled zone), it was concluded that the initial small disturbances were a valid indication of stall.

Effect of Data Averaging on Time-Varying Distortion

In figure 12 the steady-state distortion index (DPCWR) is applied on a time-variant basis for a typical wind tunnel stall point (reading 148). Although 225-milliseconds of digitized data were available before each stall, only the last 40-milliseconds (10 rotor revolutions) before stall were analyzed to reduce the amount of data processing and to allow more detailed examination of the time period near stall.

The 50-millisecond time span used in figure 12 represents a period just before and including the complete breakdown of flow in the compressor (terminal stall) and is identical to the time span used in figure 11(b) for reading 148. To compose this figure, the distortion computations were made and values plotted every 0.125 milliseconds. The critical level and its error band, along with the stall time and steady-state distortion level, are shown on the plots. Figure 12 shows increasing values of the time increment over which compressor-face pressures were averaged before computing distortion values. When time-averaging distortion data, the averaging procedure should be applied directly to the pressure data rather than to the time-varying distortion index. It is clear from figure 12(a) that if the time varying index is averaged, it will not necessarily approach the steady-state value as a limit.

The averaging time of 0.07 rotor revolution (approximately 0.25 msec) shown in figure 12(a) represents the effective averaging time of the predigitizer analog filters shown in figure 4. (More details on analog averaging are given in ref. 8.) The averaging times used in figures 12(b) through (e) represent the effects of a digital averaging procedure as well as the effects of the analog filters. For these cases the digital (i.e., arithmetic) average pressure value for each probe was determined from the digitized values encompassed by the averager "window" (of width τ) and was assigned the value of time corresponding to the center of the "window." The averager window was then moved forward by an increment of 0.125 millisecond, and the process was repeated.

As expected, increasing the averaging time τ reduces the level of the instantaneous distortion peaks, smooths the variation of distortion with time, and reduces the mean value of the fluctuations. The mean value of DPCWR approaches the steady-state level as τ approaches infinity. A more subtle effect of increasing τ is that the relative magnitudes of the distortion parameter peaks are not maintained. For example, the highest distortion peak before stall in figure 12(a) occurs at 18 milliseconds, but in figure 12(c) the highest peak occurs at 5 milliseconds. This effect is important when the response of the compressor to variations in distortion is considered.

Since the instantaneous distortion approach is simply the application of a steady-state distortion parameter on a quasi-steady-state basis, the most ideal representation of this approach would be to associate compressor stall with a single distortion peak, which has the following characteristics:

(1) It is the highest distortion peak that occurs in the span of time beginning with equilibrium engine operation and ending with the first indication of stall inside the compressor.

(2) The time increment between the highest distortion peak and the first indication of the stall should be no longer than the transport time required for the distortion to reach the stalling stage, plus the time between the origin of stall and the first indication by the interstage instrumentation, plus the time delay in blade-element response (i.e., flow separation).

(3) The amplitude of the highest instantaneous distortion peak should equal or exceed the critical level of distortion, as determined by the steady-state correlation of figure 8.

Reference 9 mentions a delay of less than 0.5 millisecond for blade element response. For the results presented in this report a period of 1 millisecond was used to represent the combination of transport time and blade-element response. As mentioned previously, the time increment between the origin of stall and the first indication of that stall could be as long as 6 milliseconds. In this investigation the first indication of stall was usually observed while the stalled zone was still rather small. It was not until some later time, when the stalled zone had grown in size, that the resulting compression wave (hammershock) affected the compressor-face total pressures. And, since the hammershock did not affect all pressure rakes at the same time (since the stalled zone was still rotating), a large increase in distortion amplitude usually resulted. This corresponds to a time of about 47 milliseconds in figure 12.

To meet the third criterion, it is necessary to time average the fluctuating component of compressor-face total pressure for a period that represents the dynamic response of the engine. The compressor would then be expected to respond to the resulting instantaneous distortions in a quasi-steady-state manner. The ratio of maximum instantaneous to critical distortion can be used to evaluate the effect of averaging time. When the ratio is 1.0, the highest level of distortion equals the critical level, and it is assumed that the steady-state stall criterion (fig. 8) can be applied.

Figure 13 is a plot of the ratio of maximum instantaneous to critical distortion as a function of averaging time for each of the seven drift stalls. The basic aspects of DPCWR have been programmed on an analog computer (ref. 10), and the results show that high levels of the parameter exist at many times before stall. But it was felt that the number of high distortion levels that existed in the 40 millisecond-period before stall were sufficient to allow a valid determination of the averaging time required to bring the peak values down near the critical level.

The square symbols (reading 148) in figure 13 represent the data from figure 12 and the steady-state distortion. Plots similar to figure 12 were available for all readings but are not shown in the report. For all seven readings the ratio of steady-state to critical distortion is represented by a solid symbol in figure 13, plotted at the value of $\tau = \infty$. The set of solid symbols shows clearly that the steady-state levels were not sufficient to cause stall, based on the correlation of figure 8.

Examination of figure 13 shows that five of the seven readings had their desired averaging times in the range of 0.2 to 0.75 rotor revolution. This amount of averaging is assumed to be an indication of the engine's dynamic response. It appears that reading 141 would have reached the desired level of peak distortion for a value of τ equal to about 1.5 rotor revolutions. This larger averaging time appeared to result from the high level of dynamic activity $\left(\overline{(\Delta P_{rms}/\overline{P})}_2 = 0.085\right)$ present at the compressor face. On the other hand, reading 164 had no instantaneous distortion values above the critical

level during the time period examined. The best single value of τ for all seven readings appears to be 0.5 rotor revolution.

Evaluation of Time-Varying Distortion for Seven Drift Stalls

Figure 14 shows one instantaneous-distortion plot for each of the drift stalls. The plots were selected based on the desired values of τ determined from the curves in figure 13. Because the data were only processed for five values of τ, the plots are for τ close to the desired value.

Time varying distortion for reading 141 is shown in figure 14(a). The critical level and its associated error band are shown in the figure. The band encompasses a large segment of the data partly because the value of $\tau = 1.18$ for this plot is somewhat less than the desired value of about 1.5 rotor revolutions. But only two of the distortion peaks shown can be related to the stall event.

A large value of distortion occurred just as stall was observed inside the compressor, at 43 milliseconds. But this distortion value is partially dependent on events that occurred after the stall was observed. In this case the averager "window" was about 4 milliseconds (1.18 rotor revolutions) wide. The distortion computed from averaged pressure values is plotted at the time corresponding to the midpoint of the window, so the peak at 43 milliseconds was influenced by pressures recorded between 41 and 45 milliseconds. As mentioned before, the effects of stall (hammershock over-pressures) did not usually appear at the compressor face until a few milliseconds after stall was observed inside the compressor. But for reading 141 the hammershock appeared at the compressor face at the same time stall was first observed inside the compressor. This could be due to the possible time delay, mentioned earlier, between the origin of stall and the initial observation of stall inside the compressor. So, instead of only being influenced by pressures recorded after stall was observed, the distortion peak at 43 milliseconds was also influenced by the hammershock. It's clear that results must be examined carefully when averaging periods exceed the time between the distortion peak and the observation of stall inside the compressor.

After considering the 1-millisecond period for transport time and blade response and the possible 6-millisecond delay between the origin and observation of stall, it is assumed that a distortion peak should be seen in figure 14(a) between about 36 and 42 milliseconds.

There is a distortion peak equal to the critical level at 36 milliseconds and another at about 39 milliseconds. Although these peaks do not represent the maximum value of distortion calculated before stall, they are of sufficient magnitude to cause stall (considering the ± 0.01 band) and they occur at times consistent with the origin of stall inside

the compressor. The large number of peaks near the critical level may mean that this index gives a statistical, rather than an explicit, indication of stall.

Figure 10(a) shows instantaneous compressor-face total-pressure contours that correspond to two of the distortion peaks in figure 14(a). These peaks occurred too early to have caused stall. However, these contours are representative of patterns observed for many other distortion peaks. They show that the peak levels of instantaneous distortion are caused by pressure contours which are more circumferential in nature than the steady-state pattern. They look like hub-radial patterns that have been stretched along a diameter. It seems clear that this stretching is related to the band of high dynamic activity in the rms contour (also fig. 10(a)).

The distortion time-history for reading 148 is shown in figure 14(b) for an averaging time of 0.31 rotor revolution, which is almost enough to bring the maximum distortion down to the critical level. Two distortion peaks (at about 34 and 37 msec) of amplitude sufficient to cause stall occurred during the 7-millisecond period before stall was observed inside the compressor. A somewhat smaller distortion peak occurred at 33.5 milliseconds, and it also could have been the cause of stall. But it occurred very early in the allowable time period and if a slightly longer averaging time had been used (to reach the desired case of maximum = critical distortion) the peak would probably fall outside of the ± 0.01 band about the critical level. (Compare figs. 12(c) and (d).) So it seems reasonable to assume that the peak at 34 or 37 milliseconds was responsible for the stall. It might seem obvious to assume that the later peak (37 msec) caused the stall. But it is possible that the peak occurred after stall had already originated inside the compressor. Stall did not affect the compressor face (via the hammershock) until much later.

The instantaneous total-pressure contours corresponding to the distortion peaks near 34 and 37 milliseconds are shown in figure 10(b). When these are compared with the steady-state contour also shown in figure 10(b), it is clear that the instantaneous patterns have much larger and less symmetric regions of low pressure. These low-pressure bulges also occurred at other circumferential locations at other times. Examination of the rms total-pressure contour in figure 10(b) again indicates that the large pressure fluctuations represented by the dark band are the probable source of the differences between steady-state and instantaneous patterns.

Reading 154 also had a steady-state hub-radial distortion pattern, and its instantaneous distortion plot is shown in figure 14(c). The distortion peak at about 32 milliseconds seems to be the obvious cause of stall. Plots for larger values of τ (not shown) indicate that this peak would remain the point of interest for a slightly larger τ necessary to bring it down to the critical level.

The maximum value of distortion for reading 154 occurred about 0.5 millisecond before the stall was observed inside the compressor. Since this would be the minimum

allowable time for transport and blade response, it is more likely that stall was caused by an earlier value of distortion that existed on the "uphill" side of the peak.

The instantaneous compressor face contour for the maximum distortion point at about 32 milliseconds is given in figure 10(c) along with the steady-state and rms pressure contours. Although the steady-state and rms contours are very similar to those of reading 148, the instantaneous contours are slightly different. But the instantaneous contours in figure 10(c) still appears to be basically a hub-radial pattern that has been stretched by the action of the band of high dynamics. The high distortion value was caused by the combination of high and low pressures in the outer annulus.

A distortion time-history and the various compressor-face pressure contours for reading 162 are shown in figures 14(d) and 10(d), respectively. For an averaging time of 0.59 rotor revolution, three distortion peaks had magnitudes close to the critical level. But based on the time stall was observed, it appears that stall was caused by a distortion that existed on the uphill side of the peak at 38 milliseconds.

Since the inlet was at $\alpha = 5^{\circ}$ for reading 162, the steady-state distortion pattern was primarily circumferential and this was also the case for the instantaneous patterns. The highest level of dynamic activity (i.e., rms level) occurred in the high pressure gradient region and resulted in an expansion and contraction of the high-pressure region. The instantaneous contour in figure 10(d) shows an expanded high-pressure region (with respect to the steady-state pattern) along with some regions below the minimum steady-state levels. A 16-millimeter film was made using a complete series of instantaneous contours from reading 162, and it showed that the major variation between contours was due to the changing extent of the high-pressure region along with occasional appearances of regions less than the minimum steady-state pressure levels.

The expansion and contraction of the high-pressure region in the film indicated that when the inlet is at angle-of-attack, the line between high- and low-pressure regions sweeps back and forth across the compressor face probes in a rather cyclic manner. A similar film was made for reading 148 ($\alpha = 0^{\circ}$), and the variation of the instantaneous pressure patterns was observed to be of a more random nature.

The operating conditions for reading 164 were very similar to those of 162, as can be seen from table I. The corrected speed was lower for reading 164, so the inlet terminal shock was farther forward. This gave a higher $\overline{P}_2/P_0$ and lower $\overline{(\Delta P_{rms}/\overline{P})}_2$. But the LSPR, and therefore the critical distortion, was about the same for both readings.

The instantaneous distortion plot for reading 164 is shown in figure 14(e), and did not involve any digital averaging. But even for this lowest averaging time, the distortion never reached the region within ± 0.01 of the critical level.

Figure 10(e) shows two instantaneous pressure contours for reading 164, and their relation to the steady-state and rms contours (same fig.) is similar to that observed for reading 162 in figure 10(d).

The ±0.01 error band about the critical level only represents a ±1σ error band for the steady-state distortion correlation of figure 8. But even if a ±3σ (±0.03) band was placed in figure 14(e), it would not include any distortion peaks. And since a ±3σ band would be expected to account for essentially all random data scatter in figure 8, it appears that the present distortion analysis is not adequate to explain this stall event.

For reading 103, vortex generators were installed on the inlet centerbody, but the steady-state distortion pattern was still basically hub-radial in nature. Figure 14(f) shows the distortion time-history for this reading using an averaging period of about one-half rotor revolution. When the previously discussed time allowances are considered, it seems probable that the distortion pattern at about 31 milliseconds was the cause of stall.

Examination of figure 10(f) shows that the instantaneous pressure contour is substantially different from the steady-state pattern and shows much greater circumferential distortion. The rms contour of figure 10(f) again shows the peak fluctuations in the region of high-pressure gradient, but the contour is less symmetric than those observed for the other cases of steady-state hub-radial distortion. It is possible that this could be a result of the vortex generators. The low-pressure region at the outer edge of the instantaneous contour corresponds to a region of low dynamic activity. But it is also near a low-pressure bulge in the steady-state pattern, which may explain why this low instantaneous pressure was observed in a region of low dynamic activity.

Figure 14(g) is the type of plot that clearly displays the basic aspect of the instantaneous distortion concept; a single peak in the distortion index which greatly exceeds all others and occurs just before engine stall. This figure is the instantaneous distortion variation for reading 261 ($\alpha = 6^{\circ}$), and the very sharp definition of the peak near 34 milliseconds is caused by an approximation in the computer program used to calculate the distortion index.

As mentioned in the definition of DPCWR, the extent functions β_{ring} only varies in increments of 60°. This means that significant errors can result for certain orientations of regions which are below the average pressure. For reading 261 the value of β_{ring} varied between 120° and 180° as the less-than-average pressure region moved back and forth across the probes. (Nearly all the distortion values plotted in fig. 14(g) correspond to the outer two rings of probes.) This stepwise fluctuation of the extent function is the cause of the sharply defined distortion peaks near 30 and 32 milliseconds, the large peak near 34 milliseconds, and some other step changes that occur at earlier times.

If the computer program had been designed to calculate the extent function in a more accurate and continuously varying manner, the results would have been quite similar to figure 14(g). However, the variation of distortion index with time would have been much smoother and the absolute values would be somewhat different. But the general features of figure 14(g) are considered to be valid.

The various total-pressure contours for reading 261 are shown in figure 10(g). The instantaneous contour corresponds to the highest distortion peak and shows an extent of

pressure below average of between 120° and 180°. Again, the high rms pressure levels occur in the region of highest steady-state total-pressure gradient.

For all of the drift stalls except reading 164, an instantaneous distortion peak of magnitude sufficient to cause stall was observed less than 7 milliseconds before the observed stall time. The 7-millisecond period was the maximum time increment that could be expected to exist between occurrence of a stall inducing pattern and the first indication of stall. The magnitude of distortion sufficient to cause stall was based on the steady-state distortion correlation (fig. 8) and its associated data scatter. To account for the data scatter, all values of distortion determined from figure 8 were assumed to include a $\pm 1\sigma$ error band of ± 0.01. More recent tests of other J85-13 engines in an altitude chamber (ref. 11) indicate that a $\pm 1\sigma$ error band much larger than ± 0.01 would be necessary to cover the scatter of data obtained from several J85-GE-13 engines.

SUMMARY OF RESULTS

An experimental investigation was conducted to determine the effect of time-varying total-pressure distortions on a J85-GE-13 engine. The engine was run behind a mixed-compression inlet in the Lewis 10- by 10-Foot Supersonic Wind Tunnel. Data were recorded from high-response total pressure probes at the compressor face. A previously developed steady-state distortion index was then applied to the digitized pressure data on an instantaneous (quasi-steady) basis, and an attempt was made to relate high levels of instantaneous distortion to compressor stall. The following conclusions were drawn:

1. Although the steady-state distortion level may be far from the predicted stall-inducing value, corresponding instantaneous distortion amplitudes can approach or exceed this value.

2. When the inlet is at zero angle-of-attack, severe total-pressure fluctuations can result in an instantaneous distortion pattern that is quite different from the steady-state pattern. For angle-of-attack cases the instantaneous distortion patterns are similar to the steady-state circumferential pattern.

3. The region of highest total-pressure fluctuations was in a band located between the high and low (steady-state) pressure recovery zones. A great deal of the variation between instantaneous pressure contours seemed to be the result of these regions of high total-pressure fluctuations.

4. It is necessary to have an accurate indication of the time stall first occurs inside the compressor to help identify the distortion that caused stall.

5. The appearance of the hammershock at the compressor face is not an accurate indication of the time stall occurs because the time delay between the first indication of stall inside the compressor and the appearance of the hammershock is not the same for all engine stalls.

6. For this J85 engine the time-varying distortion data need to be averaged for a time period on the order of 0.5 rotor revolution before the steady-state stall criterion can be applied on an instantaneous basis.

7. After applying the proper averaging period and when the data scatter of the steady-state correlation was considered, an instantaneous distortion peak of amplitude sufficient to cause stall was observed for six of the seven drift stalls less than 7 milliseconds before stall was first observed inside the compressor.

8. The existence of numerous "false indications" of stall indicate that the present parameter and instantaneous distortion approach might provide a type of statistical probability, instead of a positive indication, that stall will occur. This is caused by a lack of detailed understanding of the effects of steady-state (and, therefore, instantaneous) distortion on compressor operation, and the current necessity of using a primarily empirical approach to correlate distortion effects.

Lewis Research Center,
National Aeronautics and Space Administration,
Cleveland, Ohio, February 5, 1974,
501-24.

REFERENCES

1. Burcham, Frank W., Jr.; and Hughes, Donald L.: Analysis of In-Flight Pressure Fluctuations Leading to Engine Compressor Surge in an F-111A Airplane for Mach Numbers to 2.17. Paper 70-624, AIAA, June 1970.

2. McAulay, John E.: Effect of Dynamic Variations in Engine-Inlet Pressure on the Compressor System of a Twin-Spool Turbofan Engine. NASA TM X-2081, 1970.

3. Calogeras, James E.: Experimental Investigation of Dynamic Distortion in a Mach 2.50 Inlet with 60 Percent Internal Contraction and Its Effect on Turbojet Stall Margin. NASA TM X-1842, 1969.

4. Wasserbauer, Joseph F.; and Choby, David A.: Performance of a Bicone Inlet Designed for Mach 2.5 with Internal Distributed Compression and 40-Percent Internal Contraction. NASA TM X-2416, 1972.

5. Coltrin, Robert E.; and Calogeras, James E.: Supersonic Wind Tunnel Investigation of Inlet-Engine Compatibility. Paper 69-487, AIAA, June 1969.

6. Calogeras, James E.; Mehalic, Charles M.; and Burstadt, Paul L.: Experimental Investigation of the Effect of Screen Induced Total Pressure Distortion on Turbojet Stall Margin. NASA TM X-2239, 1971.

7. Choby, David A.; Burstadt, Paul L.; and Calogeras, James E.: Unstart and Stall Interactions Between a Turbojet Engine and an Axiaymmetric Inlet with 60-Percent Internal-Area Contraction. NASA TM X-2192, 1971.

8. Moore, M. T.; and Lucke, J. E.: A Similarity Parameter for Scaling Dynamic Inlet Distortion. Paper 73-WA/AERO-3, ASME, Nov. 1973.

9. Jansen, Willem; Swarden, Michael C.; and Carlson, Albert W.: Compressor Sensitivity to Transient and Distorted Transient Flows. Paper 71-670, AIAA, June 1971.

10. Costakis, William G.: Analog Computer Implementation of Four Instantaneous Distortion Indices. NASA TM X-2993, 1974.

11. Calogeras, James E.; Johnsen, Roy L.; Burstadt, Paul L.: Effect of Screen-Induced Total-Pressure Distortion on Axial-Flow Compressor Stability. NASA TM X-3017, 1974.

TABLE I. - INLET-ENGINE CONDITIONS FOR WIND TUNNEL STALL POINTS

Reading	Inlet configuration (a)	Steady-state distortion distortion	Free-stream Mach number, M_0	Angle of attack, α, deg	Compressor pressure ratio, $\bar{P}_2/P_0$	Compressor mass flow ratio, m_2/m_0	Corrected engine speed $(N/N^* \sqrt{\theta_2})100$, percent	Compressor pressure ratio at stall, $\bar{P}_3/\bar{P}_2$	Loss in stall compressor pressure ratio, LSPR	Predicted critical distortion	Dynamic pressure distortion, $(\Delta P_{rms}/\bar{P})_2$
141	II	Hub-radial	2.50	0	0.761	0.906	98.82	7.045	0.063	0.044	0.085
148	↓	Hub-radial	2.50	0	.788	.704	86.88	4.601	.127	.097	.066
154	↓	Hub-radial	2.50	0	.799	.834	92.25	5.240	.116	.086	.069
162	↓	180^O Circumferential	2.58	5	.769	.925	92.89	5.288	.171	.149	.046
164	↓	180^O Circumferential	2.58	5	.843	.917	86.89	4.388	.177	.157	.019
103	II-CB	Hub-radial	2.68	0	.736	.840	86.42	4.684	.111	.082	.050
261	II-CCB	180^O Circumferential	2.58	6	.783	.851	87.00	4.355	.185	.168	.021

[a] II denotes standard bleed configuration (see ref. 4); CB denotes vortex generators on centerbody; CCB denotes vortex generators on cowl and centerbody.

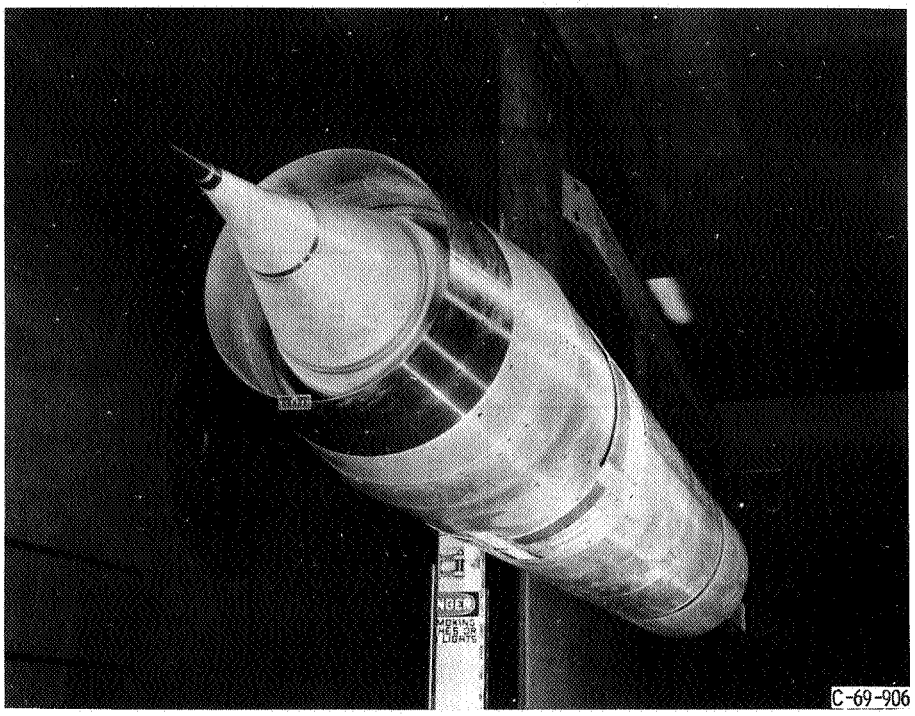

Figure 1. - Inlet-coldpipe installation in wind tunnel.

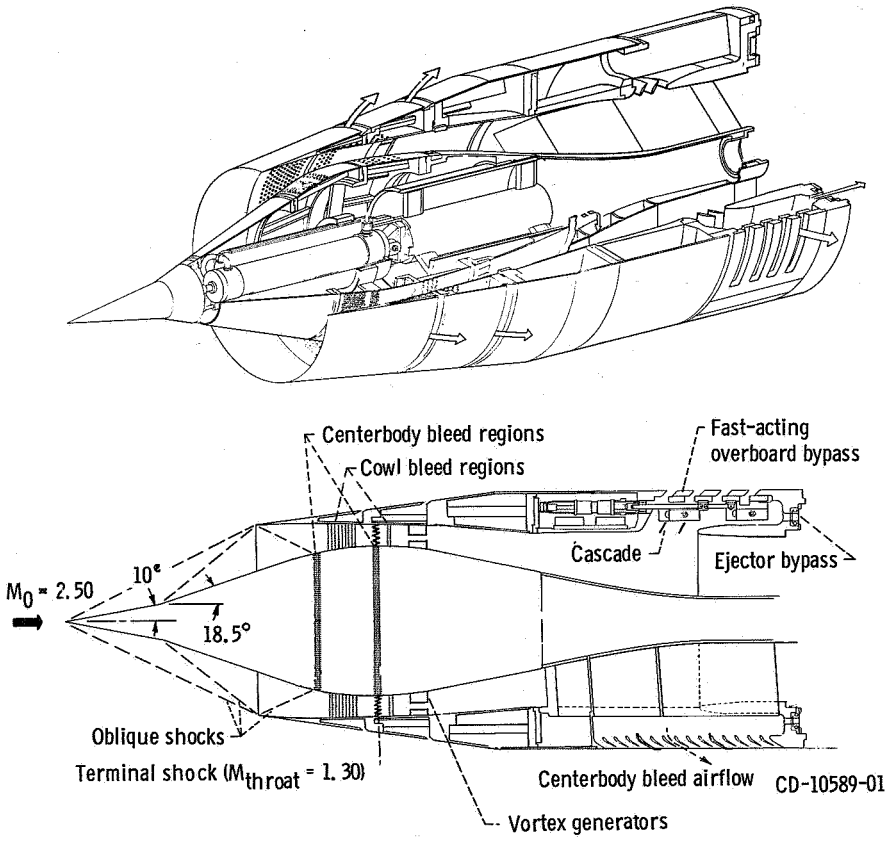

Figure 2. - Inlet details.

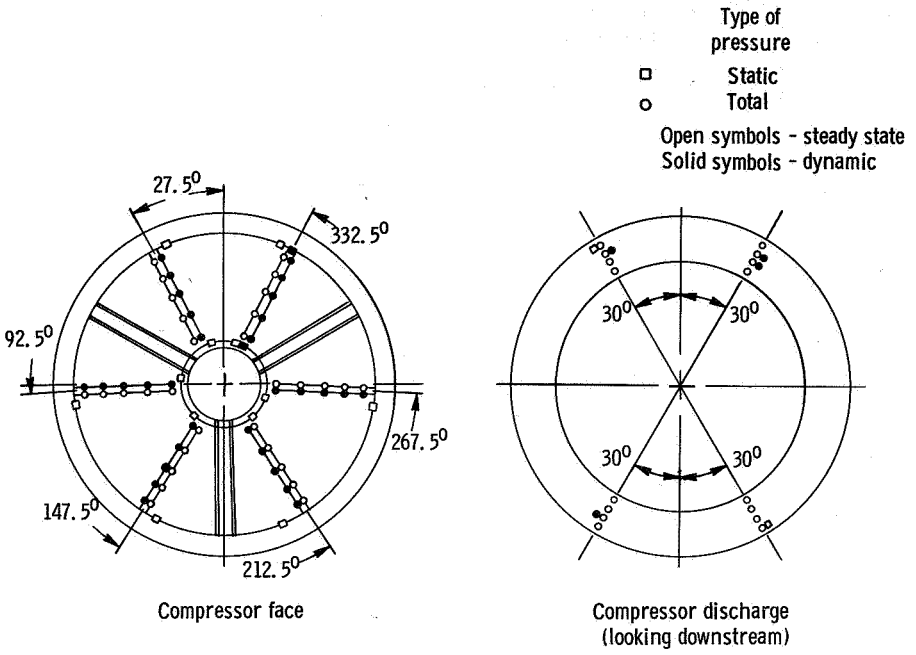

(a) Compressor face and compressor discharge measuring stations.

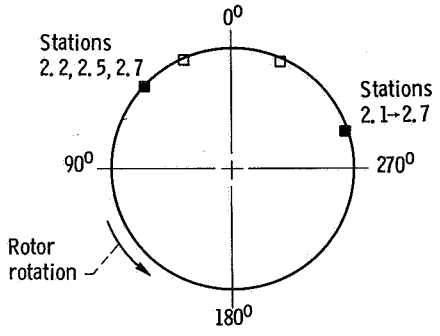

Station	Location of static taps, deg	
	Dynamic	Steady-state
2.1	290.0	22.5, 337.5
2.2	45.0, 290.0	
2.3	290.0	
2.4	290.0	
2.5	45.0, 290.0	
2.6	290.0	
2.7	45.0, 290.0	

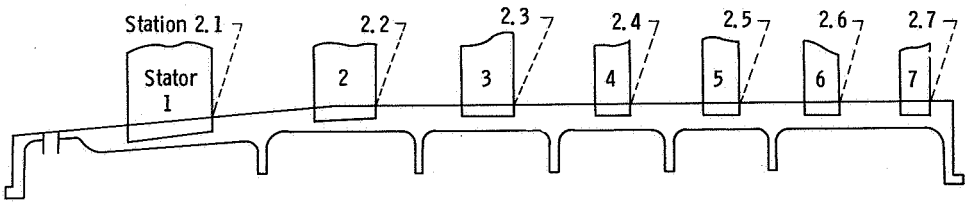

(b) Compressor interstage measuring stations.

Figure 3. - Steady-state and dynamic pressure instrumentation.

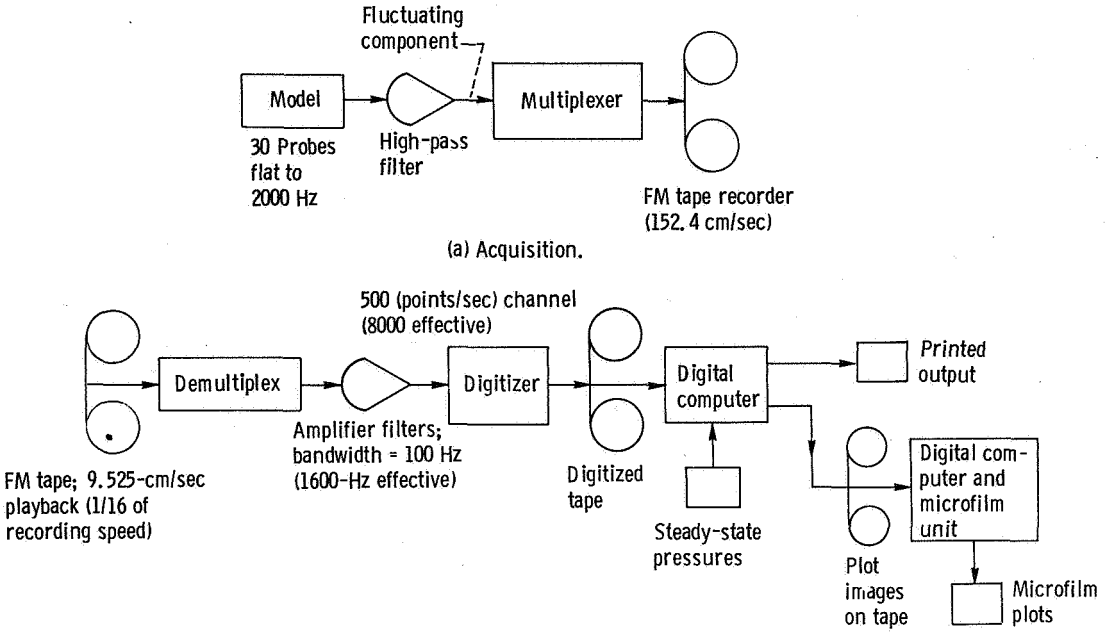

Figure 4. - Data acquisition and reduction schematics.

CS-64564

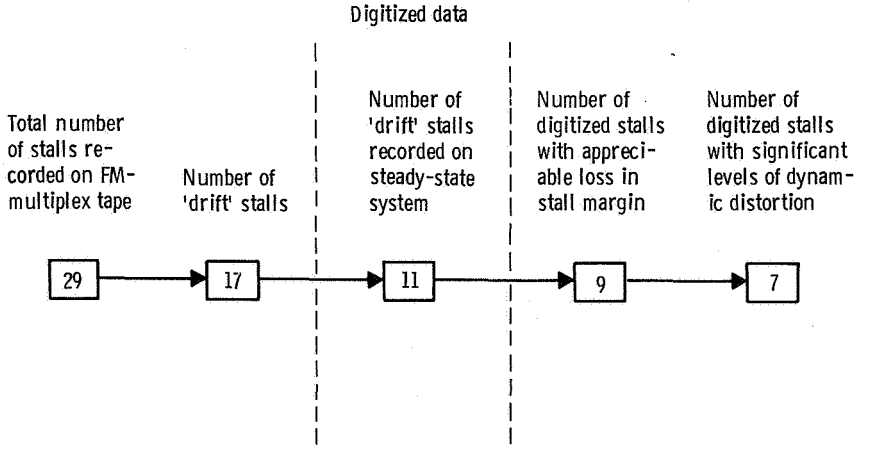

Figure 5. - Data bank resulting from 60/40 inlet-J85 engine compatibility study.

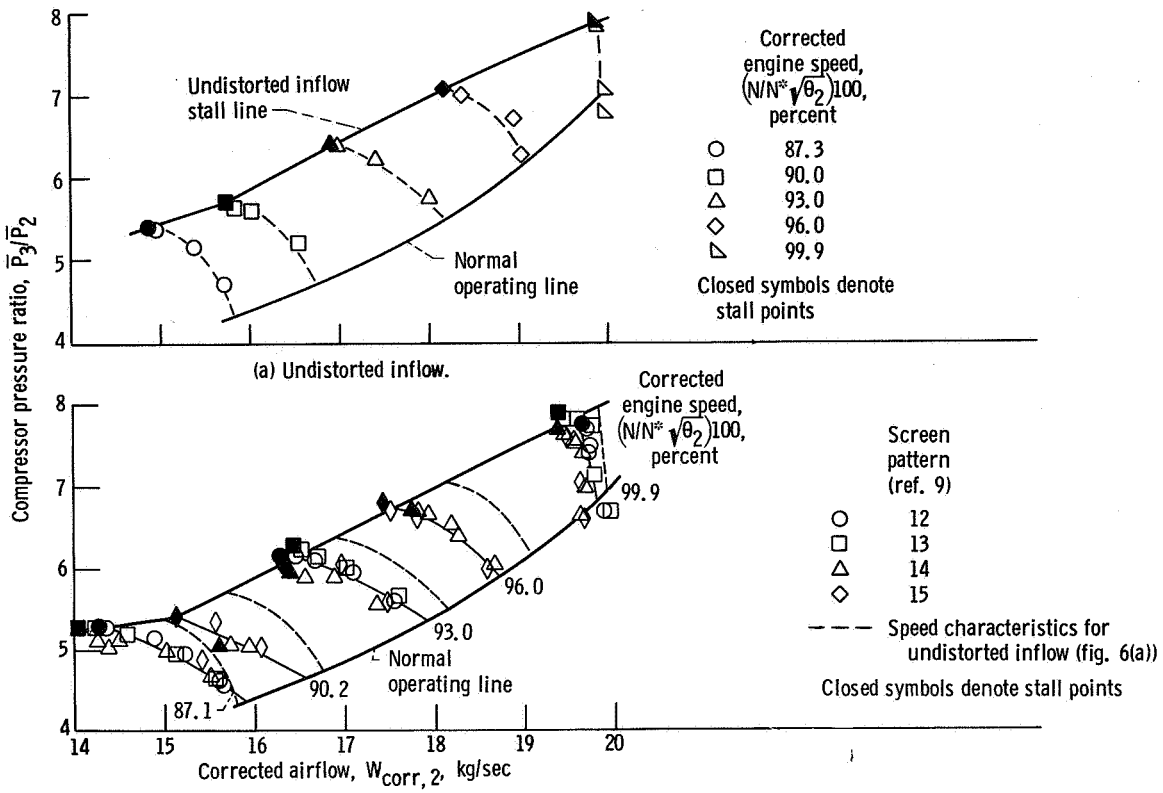

Figure 6. - Compressor performance.

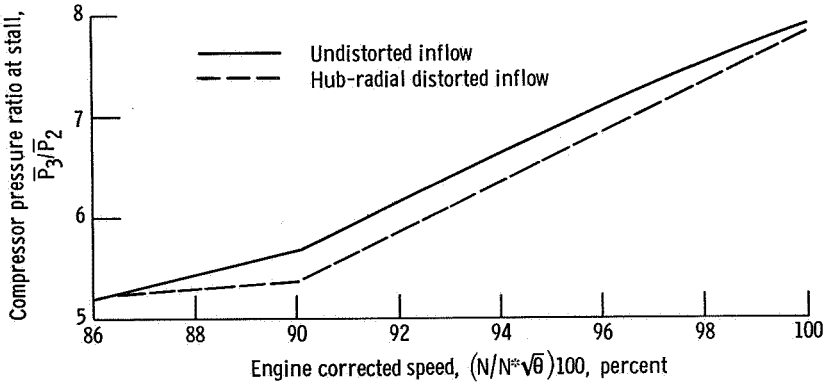

Figure 7. - Variation of stall compressor pressure ratio with engine speed.

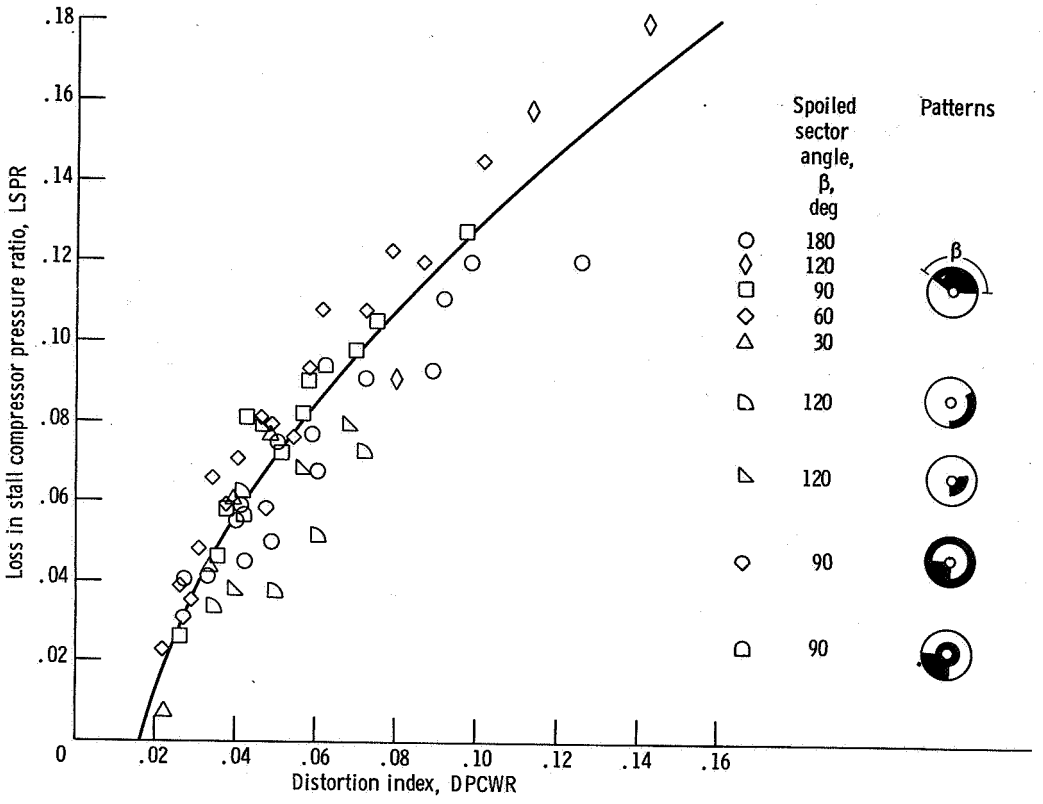

Figure 8. - Steady-state distortion correlation.

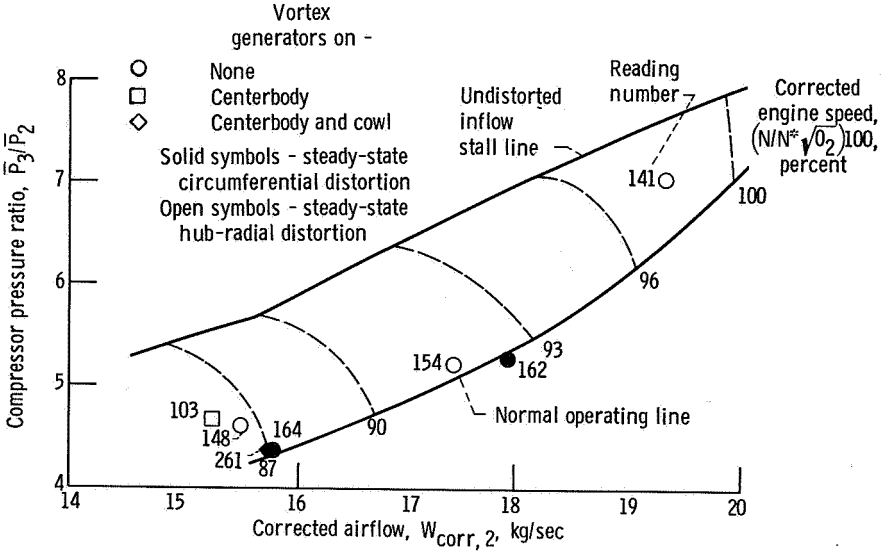

Figure 9. - Compressor operating points for "drift" stalls.

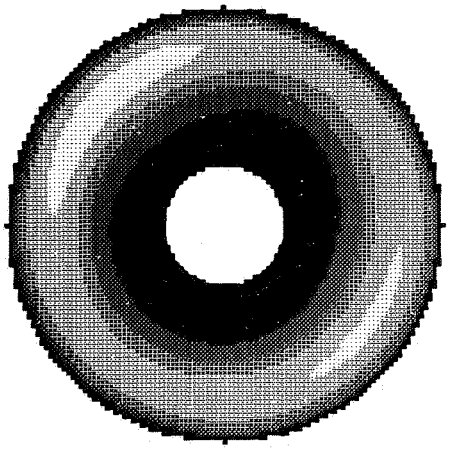

Compressor pressure ratio, P_2/P_0

0.900 TO 0.850 | 0.800 TO 0.750 | 0.700 TO 0.650
0.850 TO 0.800 | 0.750 TO 0.700 | 0.650 AND BELOW

(a-1) Steady-state total-pressure contour. Average compressor pressure ratio, $\overline{P}_2/P_0$, 0.761

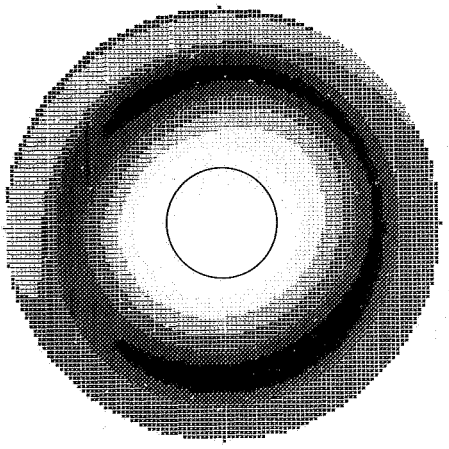

rms pressure ratio, $(\Delta P_{rms}/\overline{P})_2$

0.110 TO 0.095 | 0.080 TO 0.065
0.125 TO 0.110 | 0.095 TO 0.080 | 0.065 TO 0.050

(a-2) rms total-pressure contour. Dynamic distortion, $(\Delta P_{rms}/\overline{P})_2$, 0.085.

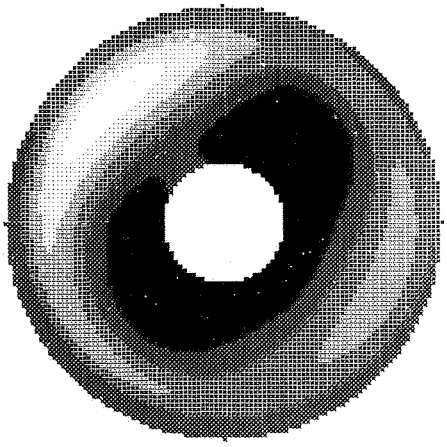

Compressor pressure ratio, P_2/P_0

0.900 TO 0.850 | 0.800 TO 0.750 | 0.700 TO 0.650
0.850 TO 0.800 | 0.750 TO 0.700 | 0.650 AND BELOW

(a-3) Instantaneous total-pressure contour. Time, 20.50 milliseconds; averaging time, 1.18 rotor revolutions.

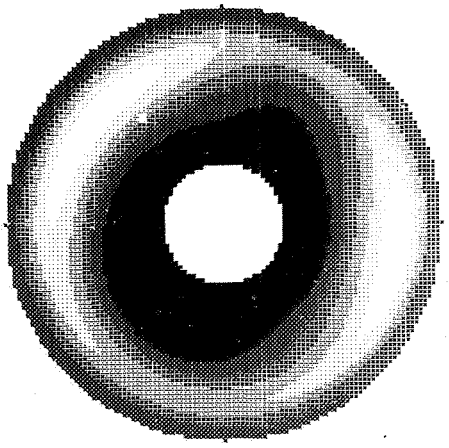

Compressor pressure ratio, P_2/P_0

0.900 TO 0.850 | 0.800 TO 0.750 | 0.700 TO 0.650
0.850 TO 0.800 | 0.750 TO 0.700 | 0.650 AND BELOW

(a-4) Instantaneous total-pressure contour. Time, 33.75 milliseconds; averaging time, 1.18 rotor revolutions.

(a) Reading 141.

Figure 10. - Steady-state, dynamic and instantaneous total-pressure contours.

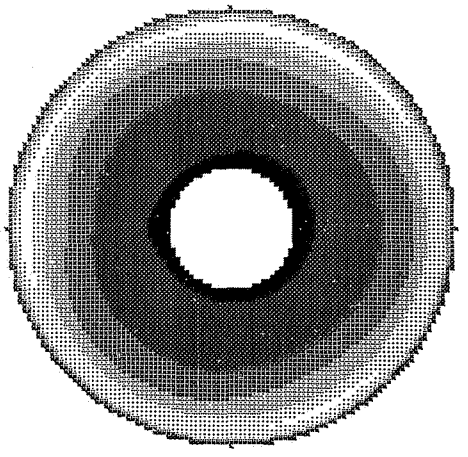

Compressor pressure ratio, P_2/P_0

0.900 TO 0.850 | 0.800 TO 0.750 | 0.700 TO 0.650
0.850 TO 0.800 | 0.750 TO 0.700

(b-1) Steady-state total-pressure contour. Average compressor pressure ratio, $\overline{P}_2/P_0$, 0.788.

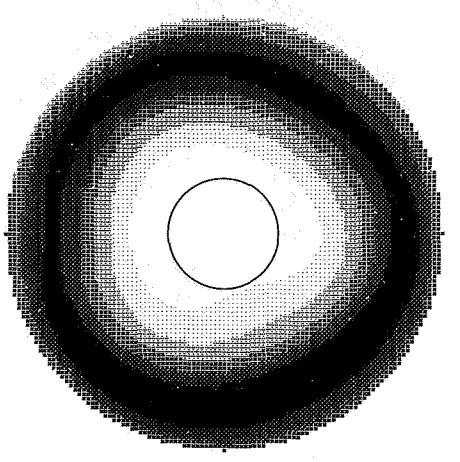

rms pressure ratio, $(\Delta P_{rms}/\overline{P})_2$

0.080 TO 0.070 | 0.060 TO 0.050
0.090 TO 0.080 | 0.070 TO 0.060 | 0.050 TO 0.040

(b-2) rms total-pressure contour. Dynamics distortion, $(\Delta P_{rms}/\overline{P})_2$, 0.066.

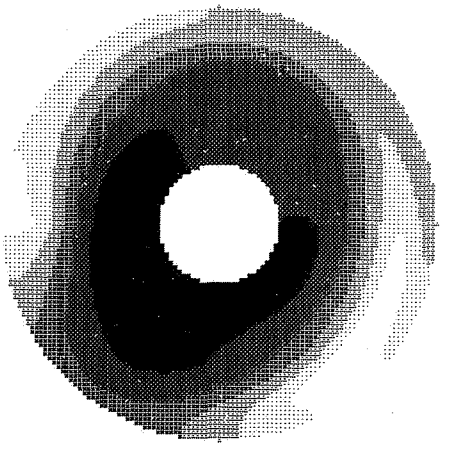

Compressor pressure ratio, P_2/P_0

0.900 TO 0.850 | 0.800 TO 0.750 | 0.700 TO 0.650
0.850 TO 0.800 | 0.750 TO 0.700

(b-3) Instantaneous total-pressure contour. Time, 33.875 milliseconds; averaging time, 0.31 rotor revolution.

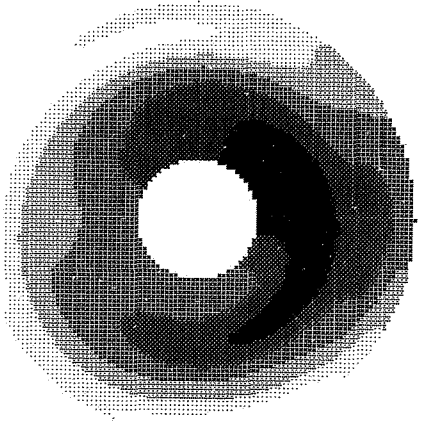

Compressor pressure ratio, P_2/P_0

0.900 TO 0.850 | 0.800 TO 0.750 | 0.700 TO 0.650
0.850 TO 0.800 | 0.750 TO 0.700

(b-4) Instantaneous total-pressure contour. Time, 37.375 milliseconds; averaging time, 0.31 rotor revolution.

(b) Reading 148.

Figure 10. - Continued.

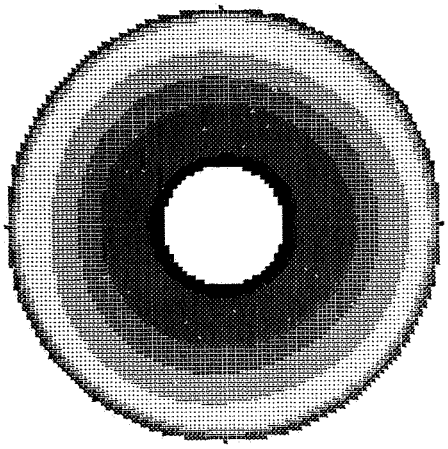

Compressor pressure ratio, P_2/P_0

0.900 TO 0.850 | 0.800 TO 0.750 | 0.700 TO 0.650
0.850 TO 0.800 | 0.750 TO 0.700

(c-1) Steady-state total-pressure contour. Average compressor pressure ratio, $\overline{P}_2/P_0$, 0.799.

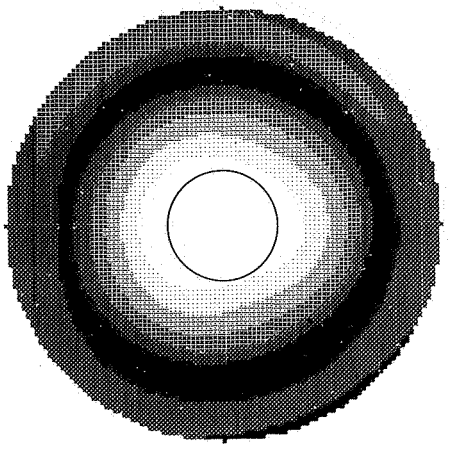

rms pressure ratio, $(\Delta P_{rms}/\overline{P})_2$

0.090 AND ABOVE | 0.080 TO 0.070 | 0.060 TO 0.050
0.090 TO 0.080 | 0.070 TO 0.060 | 0.050 TO 0.040

(c-2) rms total-pressure contour. Dynamic distortion, $(\overline{\Delta P_{rms}/P})_2$, 0.070.

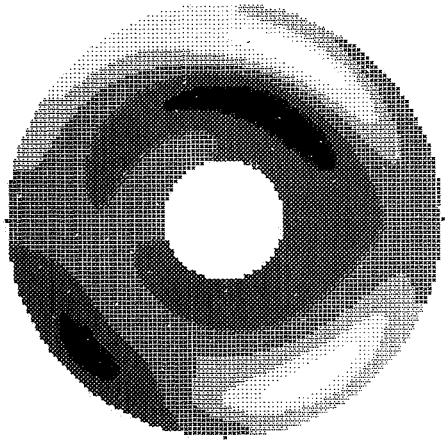

Compressor pressure ratio, P_2/P_0

0.900 TO 0.850 | 0.800 TO 0.750 | 0.700 TO 0.650
0.850 TO 0.800 | 0.750 TO 0.700

(c-3) Instantaneous total-pressure contour. Time, 32.375 milliseconds; averaging time, 0.33 rotor revolution.

(c) Reading 154.

Figure 10. - Continued.

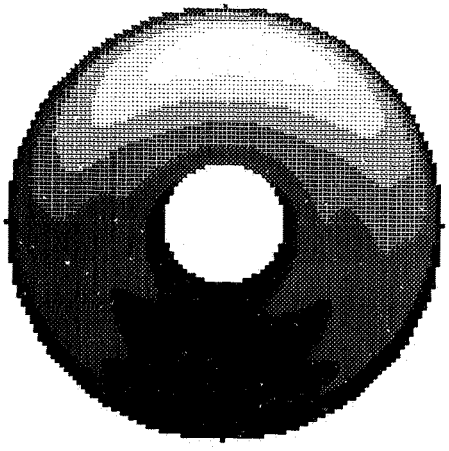

Compressor pressure ratio, P_2/P_0

0.940 TO 0.880 | 0.820 TO 0.760 | 0.700 TO 0.640
0.880 TO 0.820 | 0.760 TO 0.700

(d-1) Steady-state total-pressure contour. Average compressor pressure ratio, $\overline{P}_2/P_0$, 0.767.

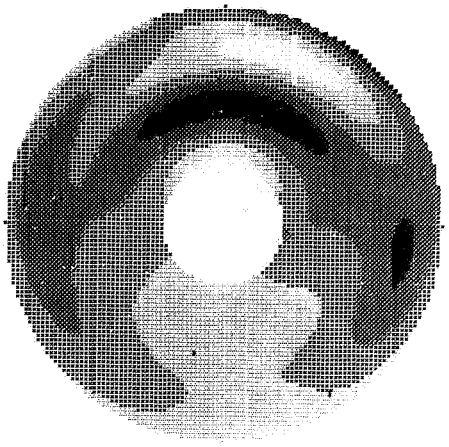

rms pressure ratio, $(\Delta P_{rms}/\overline{P})_2$

0.060 TO 0.050 | 0.040 TO 0.030
0.070 TO 0.060 | 0.050 TO 0.040 | 0.030 TO 0.020

(d-2) rms total-pressure contour. Dynamic distortion, $(\Delta P_{rms}/\overline{P})_2$, 0.046.

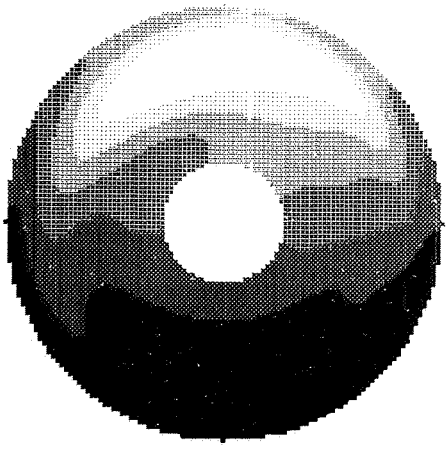

Compressor pressure ratio, P_2/P_0

0.900 TO 0.850 | 0.800 TO 0.750 | 0.700 TO 0.650
0.850 TO 0.800 | 0.750 TO 0.700 | 0.650 AND BELOW

(d-3) Instantaneous total pressure contour. Time, 37.875 milliseconds; averaging time, 0.59 rotor revolution.

(d) Reading 162.

Figure 10. - Continued.

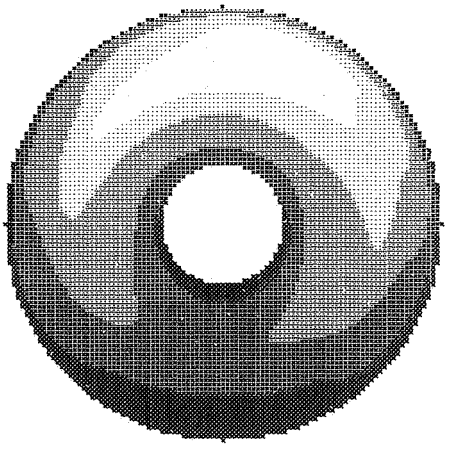

Compressor pressure ratio, P_2/P_0

0.940 TO 0.880
0.880 TO 0.820
0.820 TO 0.760
0.760 TO 0.700

(e-1) Steady-state total pressure contour. Average compressor pressure ratio, $\overline{P}_2/P_0$, 0.844.

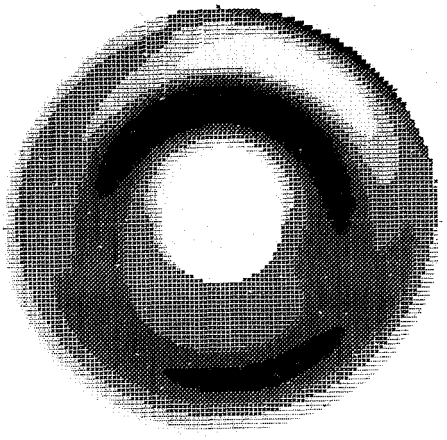

rms pressure ratio, $(\Delta P_{rms}/\overline{P})_2$

0.050 AND ABOVE
0.050 TO 0.025
0.025 TO 0.020
0.020 TO 0.015
0.015 TO 0.010
0.010 TO 0.005

(e-2) rms total-pressure contour. Dynamic distortion, $(\Delta P_{rms}/\overline{P})_2$, 0.019.

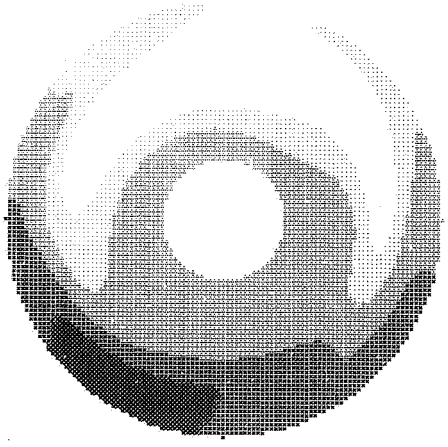

Compressor pressure ratio, P_2/P_0

0.900 TO 0.850
0.850 TO 0.800
0.800 TO 0.750
0.750 TO 0.700

(e-3) Instantaneous total-pressure contour. Time, 35.25 milliseconds; averaging time, 0.066 rotor revolution.

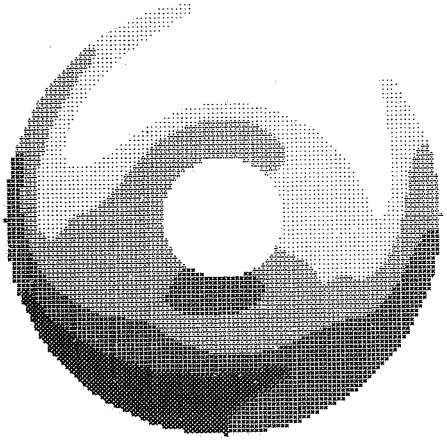

Compressor pressure ratio, P_2/P_0

0.900 TO 0.850
0.850 TO 0.800
0.800 TO 0.750
0.750 TO 0.700

(e-4) Instantaneous total-pressure contour. Time, 36.125 milliseconds; averaging time, 0.066 rotor revolution.

(e) Reading 164.

Figure 10. - Continued.

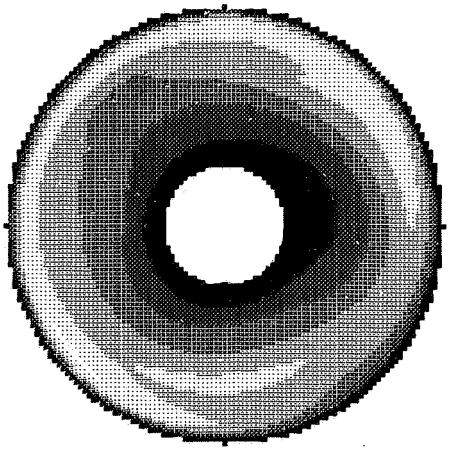

Compressor pressure ratio, P_2/P_0

0.780 TO 0.760 | 0.740 TO 0.720 | 0.700 TO 0.680
0.760 TO 0.740 | 0.720 TO 0.700 | 0.680 AND BELOW

(f-1) Steady-state total-pressure contour. Average compressor pressure ratio, $\overline{P}_2/P_0$, 0.736.

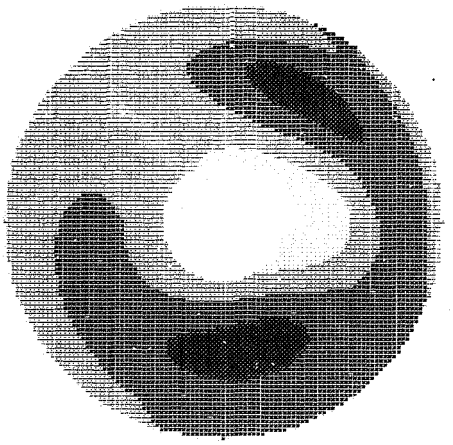

rms pressure ratio, $(\Delta P_{rms}/\overline{P})_2$

0.050 TO 0.040 | 0.070 TO 0.060
0.040 TO 0.030 | 0.060 TO 0.050

(f-2) rms total-pressure contour. Dynamic distortion, $(\Delta P_{rms}/\overline{P})_2$, 0.050.

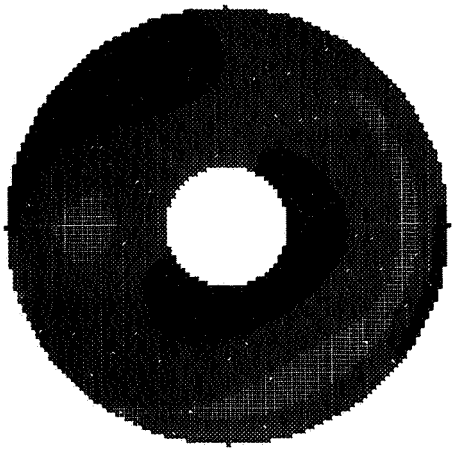

Compressor pressure ratio, P_2/P_0

0.820 TO 0.760 | 0.700 TO 0.640
0.760 TO 0.700

(f-3) Instantaneous total-pressure contour. Time, 32.125 milliseconds; averaging time, 0.55 rotor revolution.

(f) Reading 103.

Figure 10. - Continued.

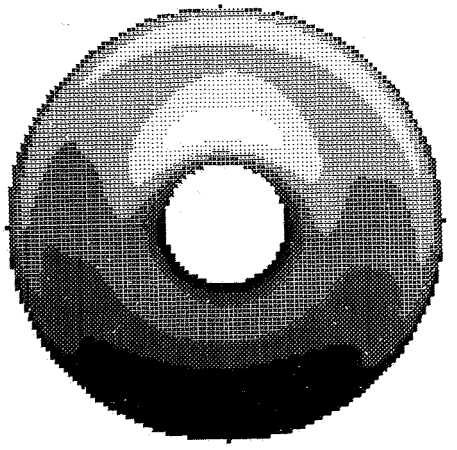

Compressor pressure ratio, P_2/P_0

0.900 TO 0.850 | 0.800 TO 0.750 | 0.700 TO 0.650
0.850 TO 0.800 | 0.750 TO 0.700 | 0.650 AND BELOW

(g-1) Steady-state total-pressure contour. Average compressor pressure ratio, $\overline{P}_2/P_0$, 0.783.

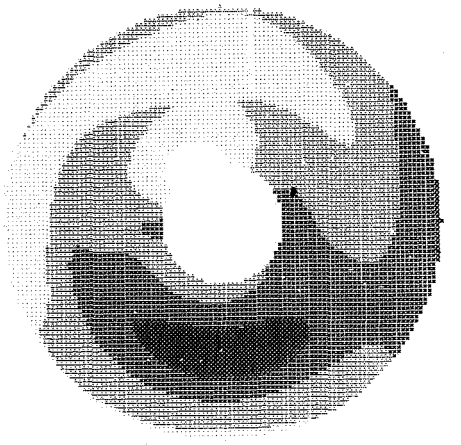

rms pressure ratio, $(\Delta P_{rms}/\overline{P})_2$

0.045 TO 0.035 | 0.025 TO 0.015
0.035 TO 0.025 | 0.015 TO 0.005

(g-2) rms total-pressure contour. Dynamic distortion, $(\Delta P_{rms}/\overline{P})_2$, 0.021.

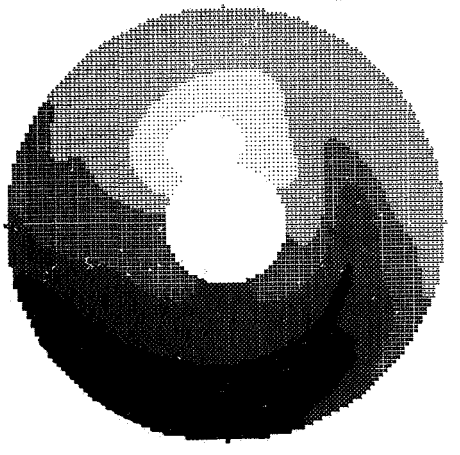

Compressor pressure ratio, P_2/P_0

0.900 TO 0.850 | 0.800 TO 0.750 | 0.700 TO 0.650
0.850 TO 0.800 | 0.750 TO 0.700 | 0.650 AND BELOW

(g-3) Instantaneous total-pressure contour. Time, 33.250 milliseconds; averaging time, 0.19 rotor revolution.

(g) Reading 26.

Figure 10. - Concluded.

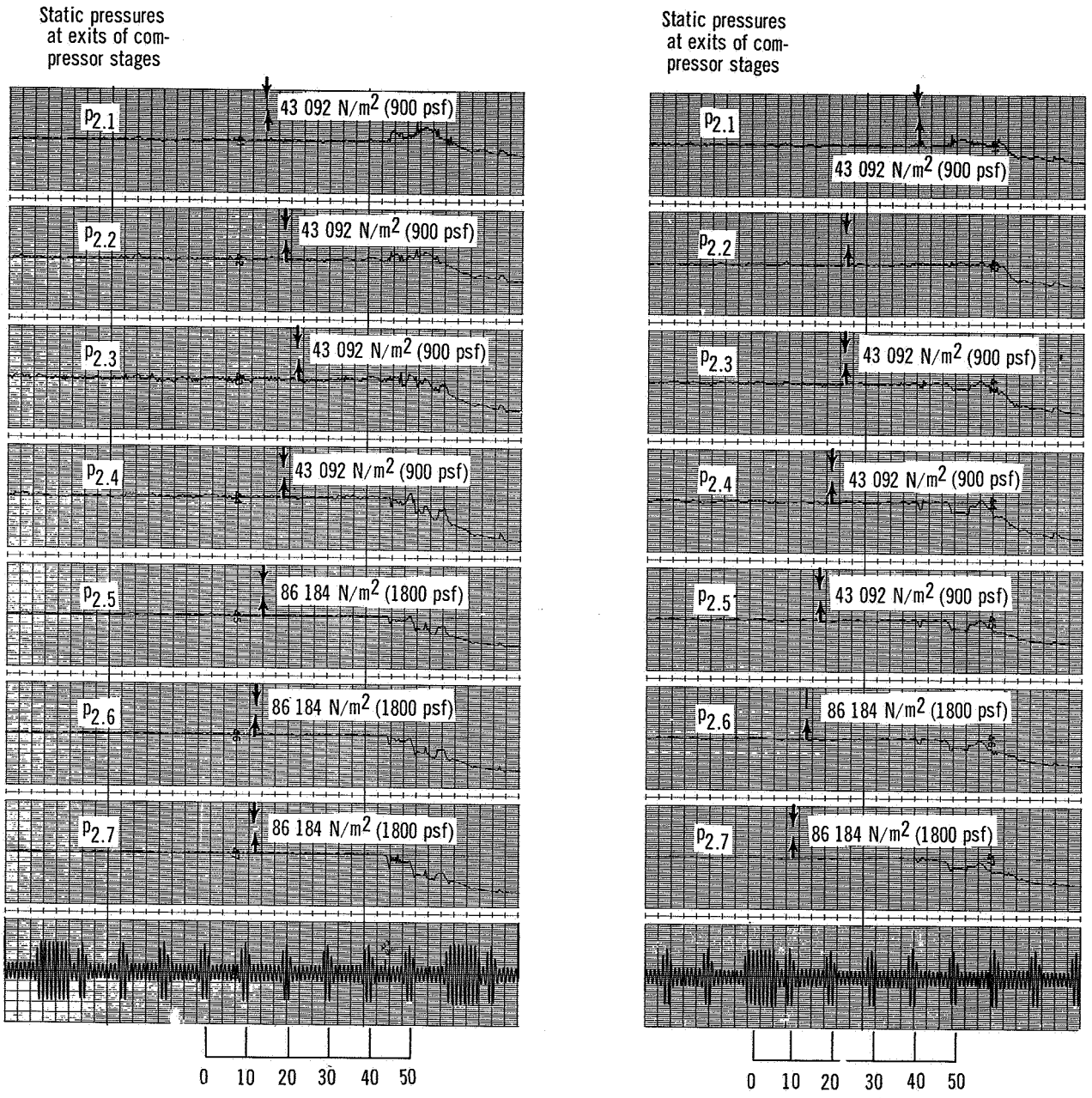

(a) Reading 141.

(b) Reading 148.

Figure 11. - Static pressures inside compressor.

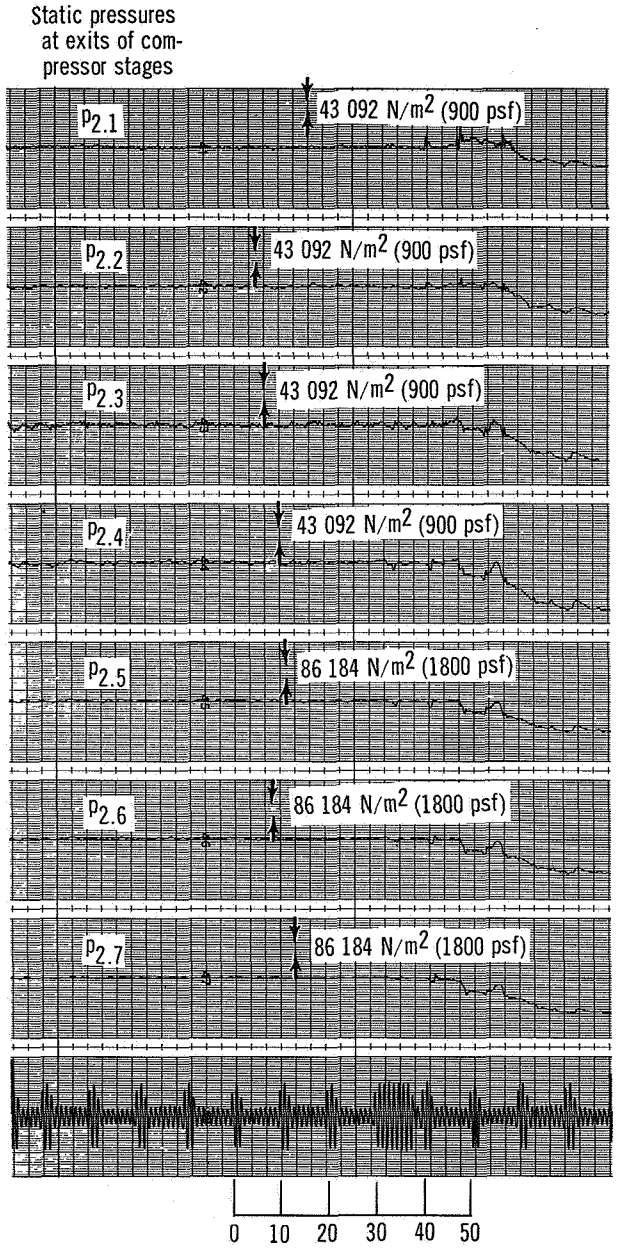

(c) Reading 154.

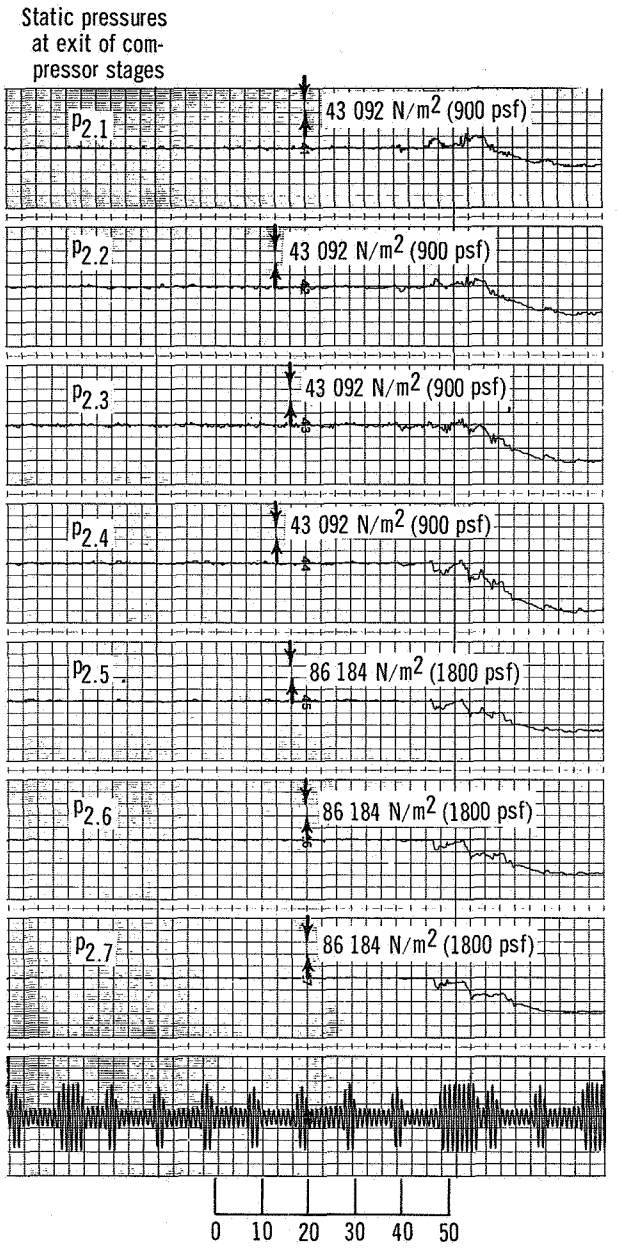

(d) Reading 162

Figure 11. - Continued.

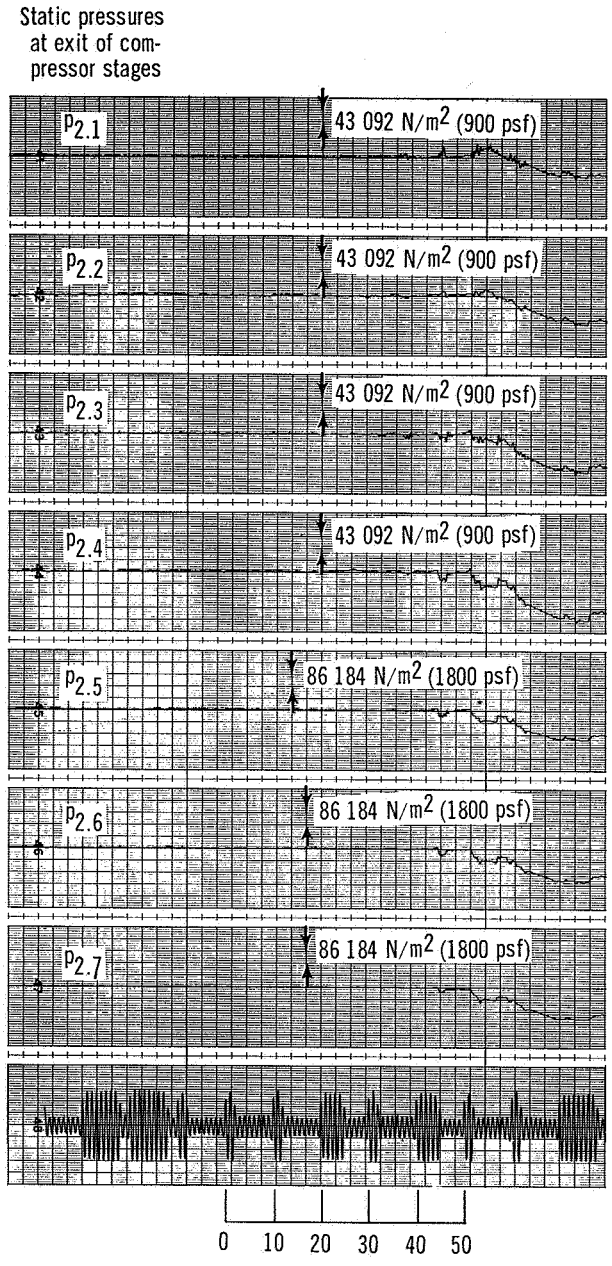

(e) Reading 164.

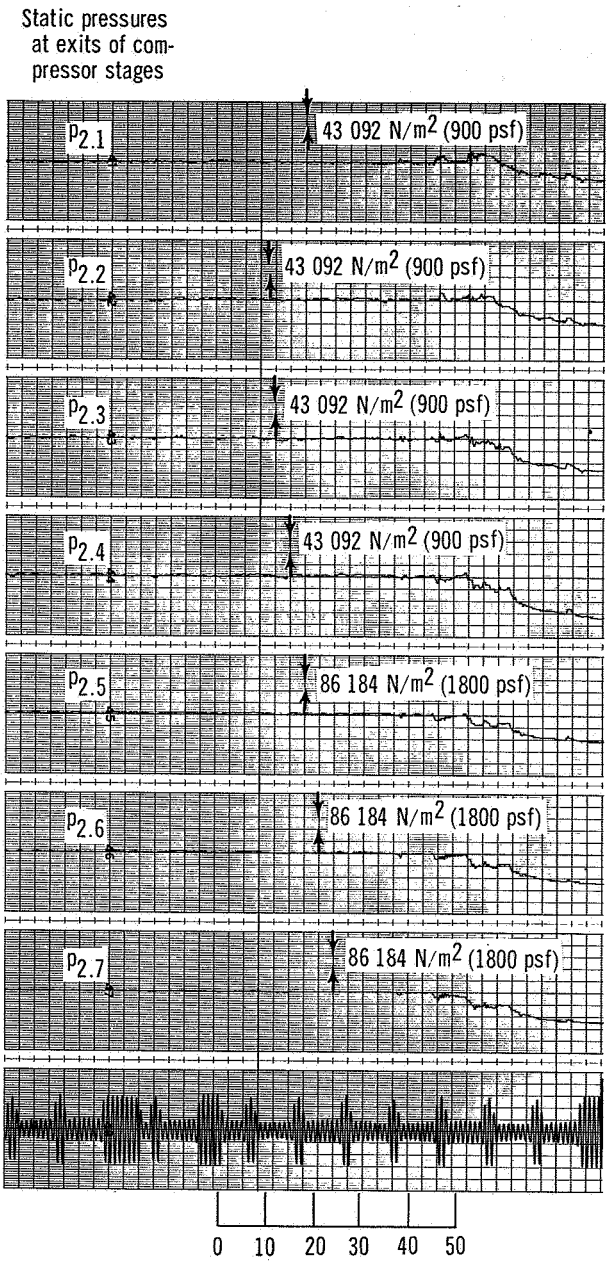

(f) Reading 103.

Figure 11. - Continued.

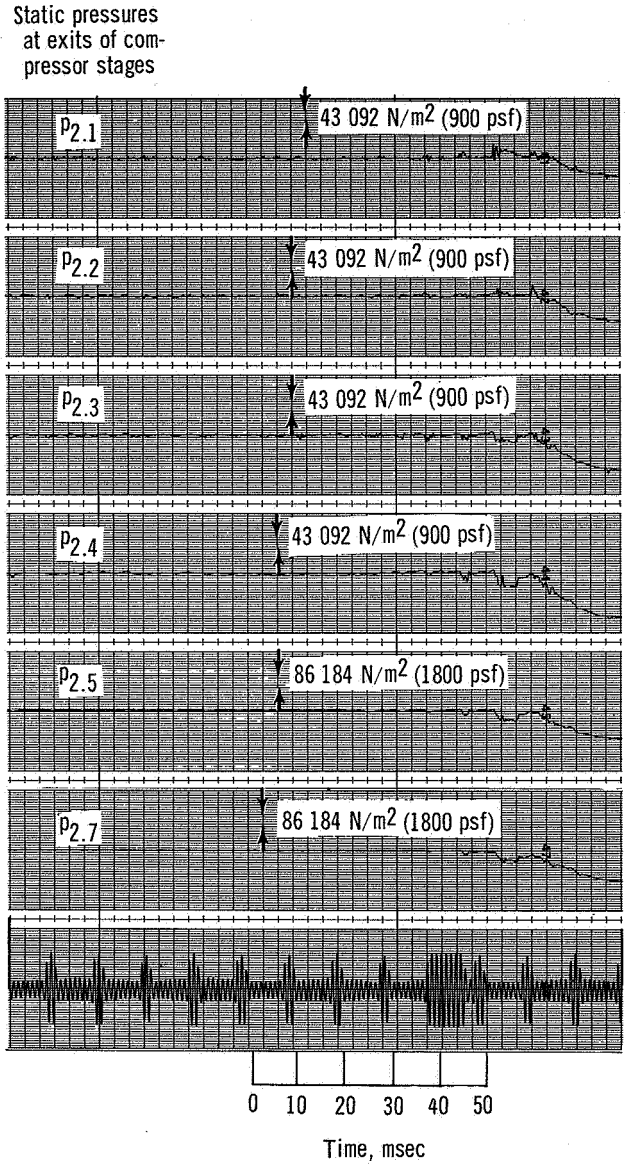

(g) Reading 261.

Figure 11. - Concluded.

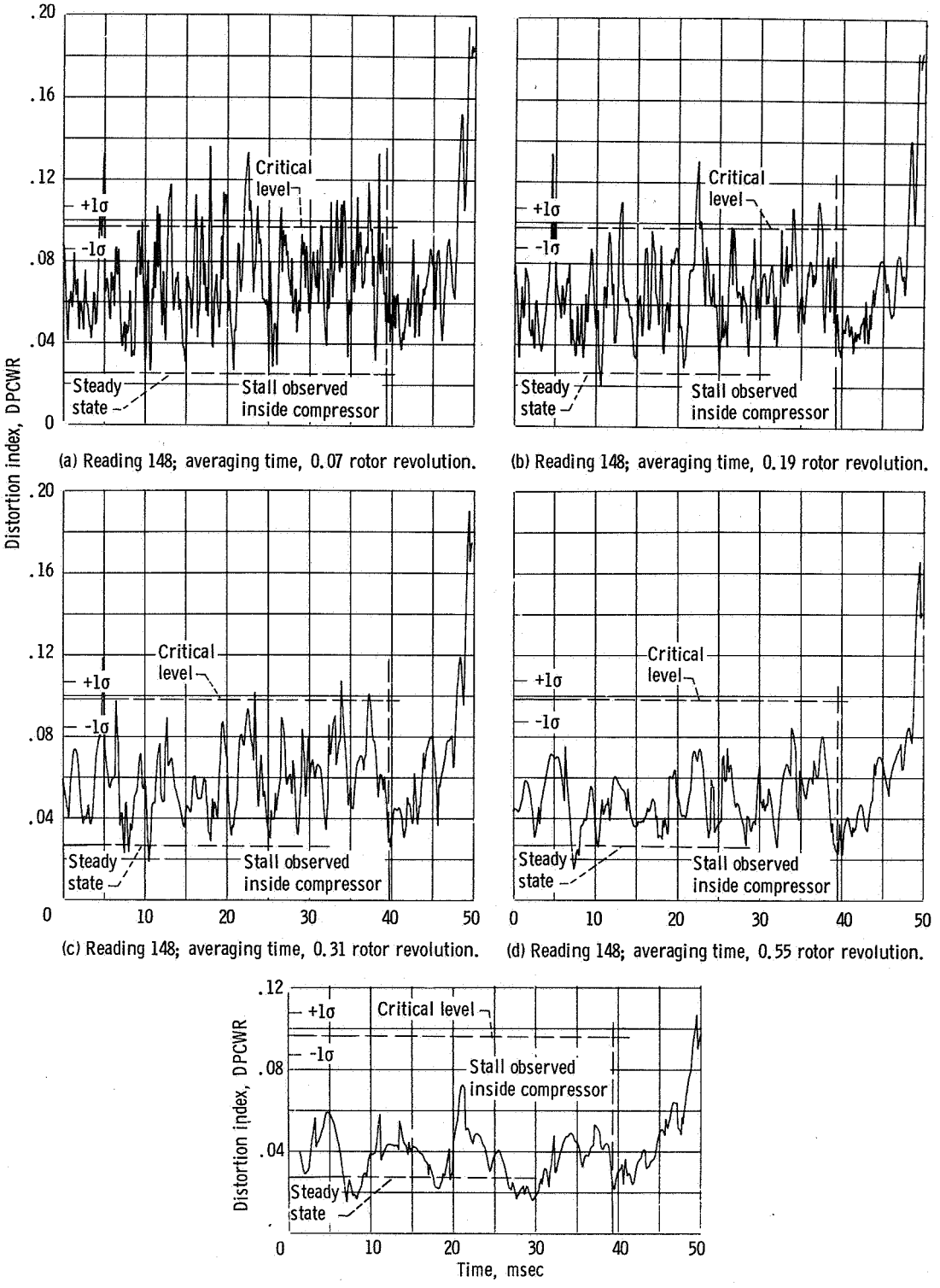

(a) Reading 148; averaging time, 0.07 rotor revolution.

(b) Reading 148; averaging time, 0.19 rotor revolution.

(c) Reading 148; averaging time, 0.31 rotor revolution.

(d) Reading 148; averaging time, 0.55 rotor revolution.

(e) Reading 148; averaging time, 1.03 rotor revolutions.

Figure 12. - Effect of averaging on time-varying distortion.

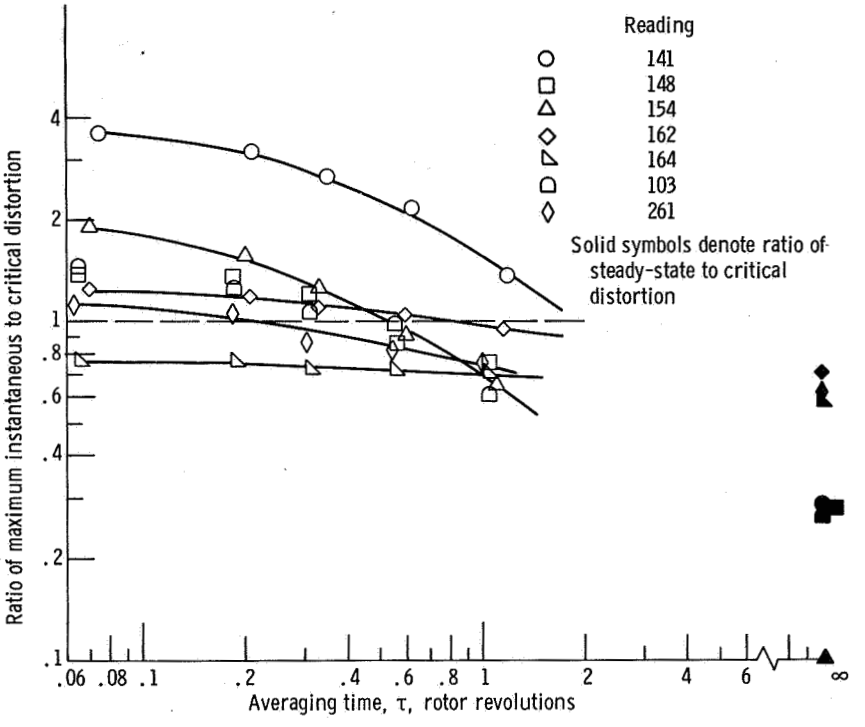

Figure 13. - Effect of averaging time on peak distortion.

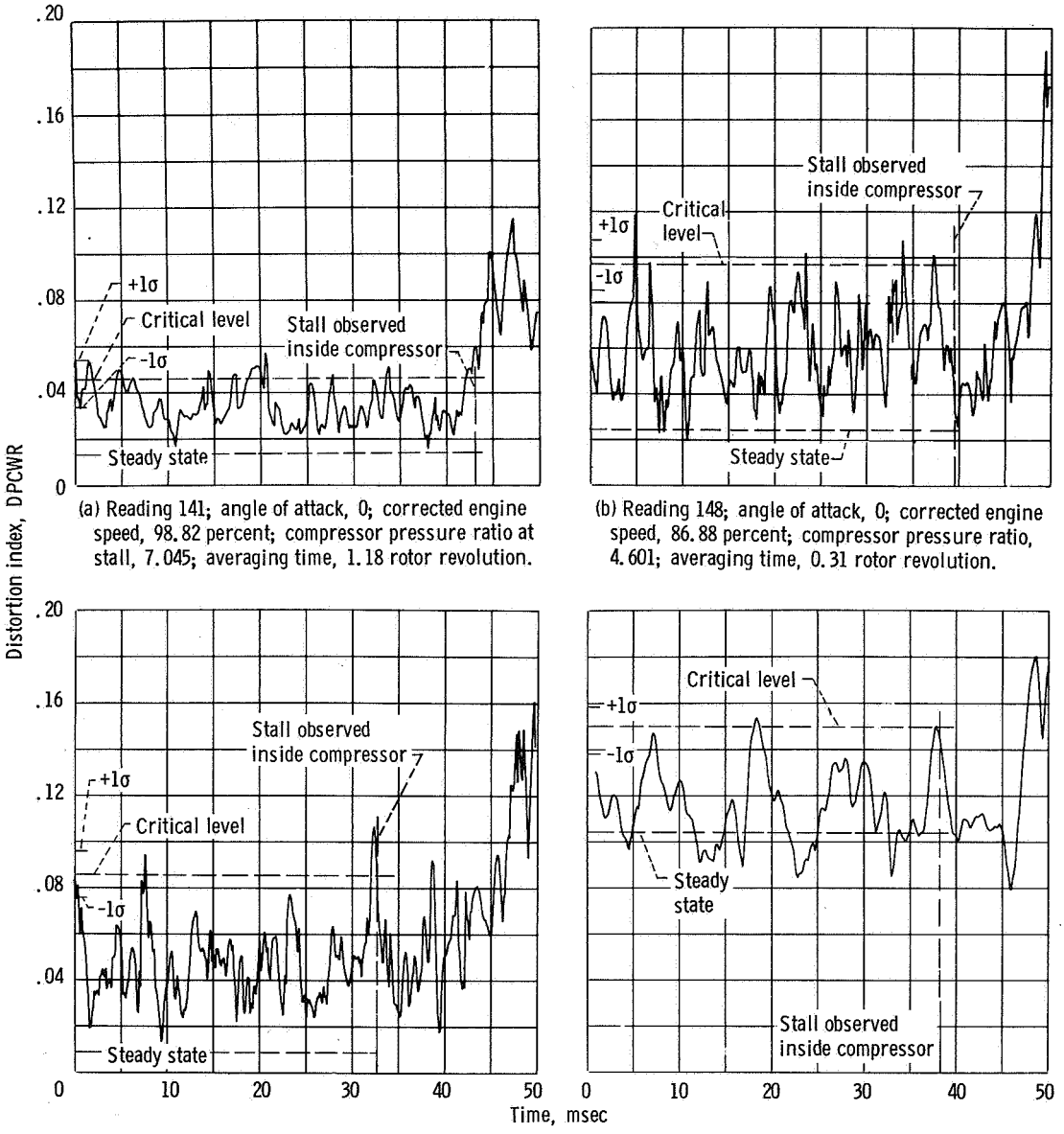

(a) Reading 141; angle of attack, 0; corrected engine speed, 98.82 percent; compressor pressure ratio at stall, 7.045; averaging time, 1.18 rotor revolution.

(b) Reading 148; angle of attack, 0; corrected engine speed, 86.88 percent; compressor pressure ratio, 4.601; averaging time, 0.31 rotor revolution.

(c) Reading 154; angle of attack, 0; corrected engine speed, 92.25 percent; compressor pressure ratio at stall, 5.240; averaging time, 0.33 rotor revolution.

(d) Reading 162; angle of attack, 5°; corrected engine speed, 92.89 percent; compressor pressure ratio at stall, 5.288; averaging time, 0.59 rotor revolution.

Figure 14. - Time-varying distortion for wind tunnel stall points.

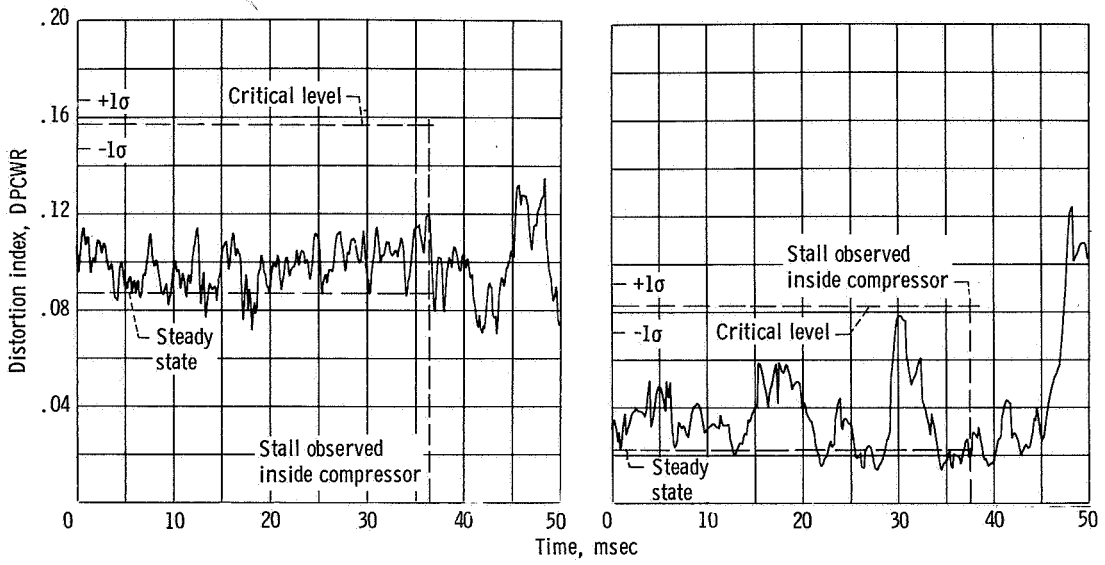

(e) Reading 164; angle of attack, 5°; corrected engine speed, 86.89 percent; compressor pressure ratio at stall, 4.388; averaging time, 0.07 rotor revolution.

(f) Reading 103; angle of attack, 0; corrected engine speed, 86.42 percent; compressor pressure ratio at stall, 4.684; averaging time, 0.55 rotor revolution.

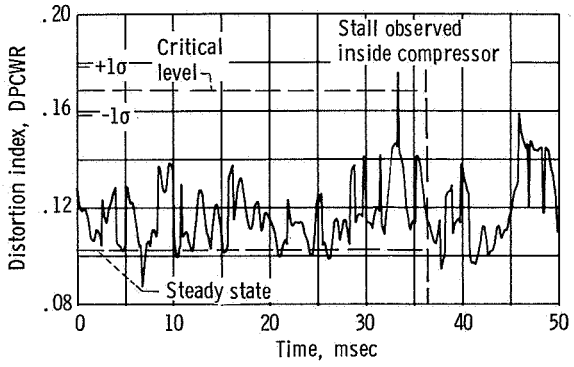

(g) Reading 261; angle of attack, 6°; corrected engine speed, 87.00 percent; compressor pressure ratio, 4.355; averaging time, 0.19 rotor revolution.

Figure 14. - Concluded.